Exploring the Methodology and Distribution of Fe Ligands in Ocean

Dr. Sherain N Al-Subiai
Visiting Scientist, MIT
Research Scientist, Kuwait Institute for Scientific Research

Faculty host at MIT
Prof. Edward Boyle
Trace Metals Research Group
Atmospheric and Planetary Sciences
Massachusetts Institute of Technology

Scholarly Exchange Fellowship
Kuwait-MIT Center for Natural Resources and the Environment
August , 2014

Table of Contents

1. Abstract

It is well established that iron (Fe) is essential for all living organisms and its availability controls phytoplankton productivity, community structure, and ecosystem functioning in vast regions of the global ocean (approx. 40%). The atmospheric Fe deposition (as volcanic ash or mineral dust) has the potential to influence the climate of the earth through affecting the level of atmospheric CO_2 uptake via phytoplankton growth (Buessler et al., 2012; Smetacek et al., 2012). However, not all Fe dust particles are bioavailable in the surface water column, only soluble Fe is bioavailable to photosynthetic aquatic organisms. Ito and Feng (2010) have reported that fine dust particles may yield higher amount of dissolved Fe in comparison to large particles due to possible variations in chemical mixing state of alkaline dust with iron-containing minerals. Previous studies have also showed that atmospheric processing mineral aerosols resulted from anthropogenic pollutants represent a significant source of bioavailable Fe solubility in the surface of the open ocean. In order to understand what controls global marine primary production, we must also understand the distribution and complexation of trace metals in seawater. Dissolved metals can be found in different chemical forms in seawater: free metal, inorganic complexes and organic complexes. The chemical speciation of a metal determines its bioavailability and biological effect, as free metal is the bioavailable form of metals (Brand et al., 1986). In the ocean, strong organic metal ligands effectively control the metals' chemical speciation because of their extremely high binding strength to metals which lead in reducing the concentrations of inorganic and free metal species. Kuwait seawater is one of the most understudied regions in the Persian Gulf for trace metals, with no reports on trace metal ligands measurements. In order to establish solid background information for Fe complexation in Kuwait seawater, Fe ligand analysis methods in the ocean was considered an essential step. With the great help from Professor Edward Boyle and Dr. Jessica Fitzsimmons (post-doc) from MIT Chemical Oceanography Trace Metals Group at Earth Atmospheric and Planetary Sciences (EAPS), we have managed to achieve 2 main targets of the planned investigation for the scientific visit: 1- Establishing the best methodologies for Fe ligands analysis in ocean; 2- Investigating the profile of Fe ligands from subtropical North Pacific.

2. Introduction

Trace metals like Fe, Zn, Cd and Co have a key biochemical functions in the enzymatic systems of the marine phytoplankton spite their very low concentrations in seawater (Morel and Price, 2003). The chemical speciation (Figure 1) of a metal determines its bioavailability and biological effect, as free metal is the bioavailable form of metals (Brand et al., 1986). However in the ocean strong organic metal-chelating ligands effectively control the metals' chemical speciation. Their extremely high binding strength to metals (K), cause limitation in the concentrations of inorganic and free metal species. There are two possible hypothesis for the function mechanisms of these ligands, either they work as a detox mechanism by lowering the bioavailable concentrations of toxic levels of some metals, or as an acquisition mechanism by enhancing the solubility of nutrient metals that would otherwise precipitate out of solution (Bruland, 1989).

These ligands have been reported previously in open ocean regimes (e.g. Rue and Bruland, 1997; Saito et al., 2001) coastal waster (Buck and Bruland, 2005) and rivers (Hoffman et al., 2007). Thus, understanding the complexation of these ligands in seawaters is important to study the metals' effect on photosynthesis, ranging from growth enhancing to biolimitation (Sunda 2013), affecting carbon uptake, and ultimately allowing for a possible use of metal fertilization as a way to help global climate mitigation (Hong et al., 2005).

Among trace metals, Fe has been widely studied because of the Fe requirement for phytoplankton productivity, community structure, and ecosystem functioning in vast regions of the global ocean (approx. 40%; Figure 1). The atmospheric Fe deposition (as volcanic ash or mineral dust) has the potential to influence the climate of the earth through affecting the level of atmospheric CO2 uptake via phytoplankton growth (Buessler et al., 2012; Smetacek et al., 2012). However, not all Fe dust particles are bioavailable in the surface water column, only soluble Fe is bioavailable to photosynthetic aquatic organisms. Ito and Feng (2010) have reported that fine dust particles may yield higher amount of dissolved Fe in comparison to large particles due to possible variations in chemical mixing state of alkaline dust with iron-containing minerals. Previous studies have also showed that atmospheric processing mineral aerosols

resulted from anthropogenic pollutants represent a significant source of bioavailable Fe solubility in the surface of the open ocean. In order to understand what controls global marine primary production, we must also understand the distribution and complexation of trace metals in seawater. Fe is reported to be complexed by ligands that can relate to some specific chemical compounds in coastal waters (Gledhill et al., 2004; Mawji et al., 2011; Velasquez et al., 2011). Recently, organic complexation was reported to dominate Fe speciation in a full-depth-profile cross-section of the North Atlantic via a combination of a stronger ligand L1 and a weaker ligand L2, hinting to phytoplankton and other sources deeper in the water column (Buck, 2013).

With this background we have pursued the following research projects:

- An exploration of dissolved Fe using Fe-binding ligands in the North Atlantic Ocean
- ALOHA temporal variability of Fe-binding ligands

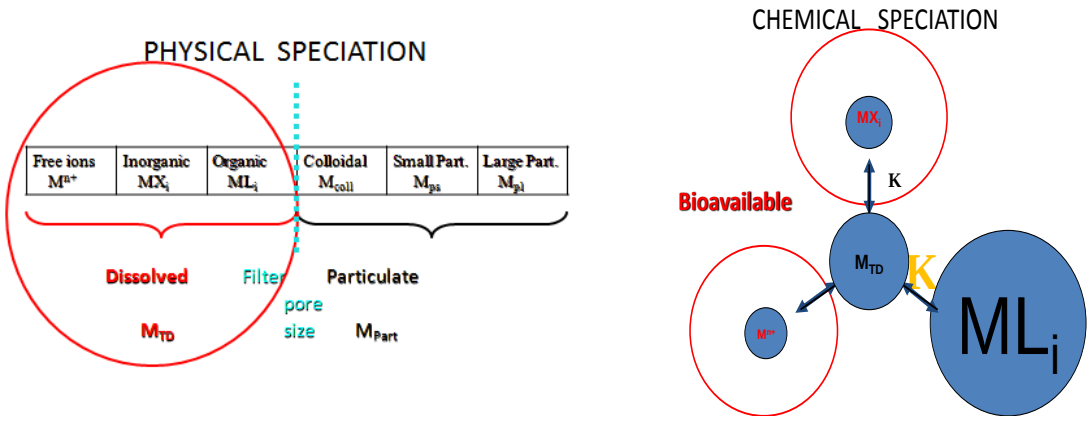

Figure 1. Physical and chemical speciation of dissolved metals

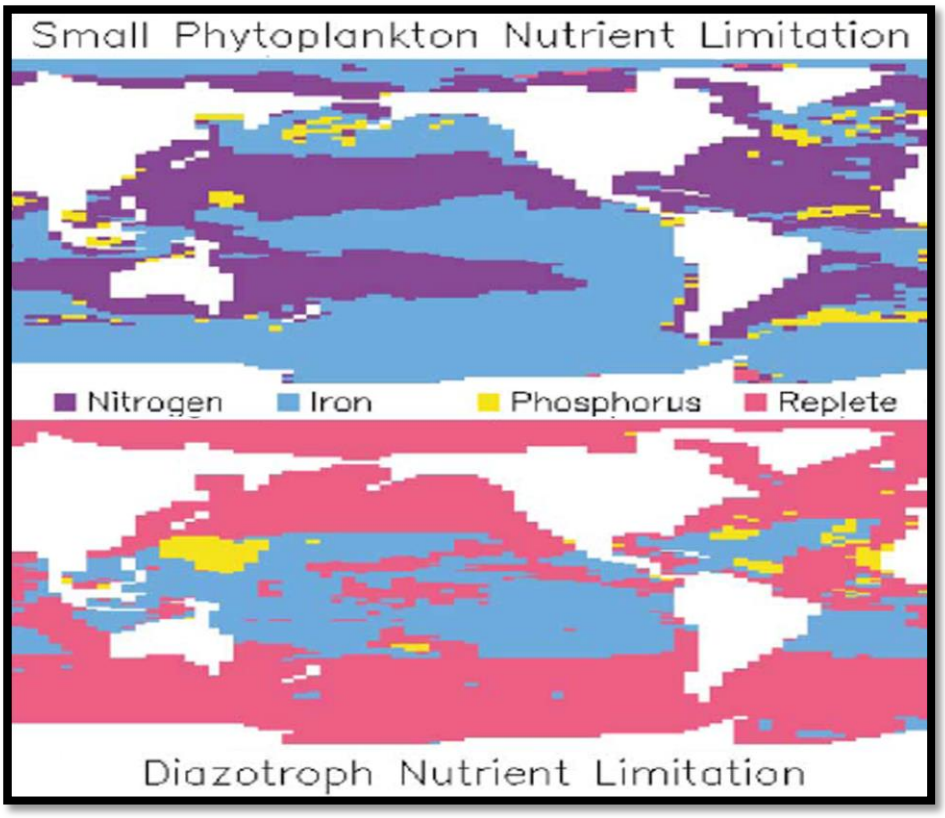

Figure 2. Cellular nutrient requirements of microorganisms (Moore *et al* 2002)

3. Standardization of the cathodic stripping voltammetry (CLE-ACSV) protocol

At the beginning we could not get the accurate baseline, we were unable to get a growing Fe peak around -450 mV. We tried to check every single step in our procedure to standardize our protocol. We have felt that there must be an electrode problem and its probably with Pt electrode instead of reference electrode as the later would change the position of the peak not its height. We turned off both instruments (analyzer and the CGME), and carefully unplug and replug each and every cord attached to the instruments. Then, the Pt electrode was wiped MANY times with clean MeOH, and rinsed off very carefully with pH 2 until it's clean. Also we dropped a Hg drop one at a time and observed the size to ensure (at least visually) that the Hg drop appears to be exactly the same size each time. The data was still looked bad, peaks were in a good shape but the height was decreasing with increasing Fe added which was strange (Figure 3A). We started to think about if there is anything wrong with standard, however to save our resources and time we have preferred to evaluate all other parameters before moving on to that stage. Given that the peaks are in perfect shape at perfect voltage, and the CGME is working reliably; we don't see what else it could be except 2 probability: either the initial sample are contaminated and somehow we are getting them cleaner as the titrations go on (compensating for the added Fe) or the Teflon vials are not equilibrated probably and the ammonia buffer is not clean. We have rinsed all vials with 3 times with pure water and equilibrated them overnight with appropriate addition of Fe standards. Also, old buffer was replaced with clean borate buffer (4N NH_4OH + borate buffer). We managed to get no peak at all in the +0 (blank) with good linearity (Figure 3B). Test seawater was used 3 times and the three runs were nearly identical; and the procedure is ready to go and apply for Fe-binding ligands. The full CLE-ACSV procedure is attached in the appendix (I).

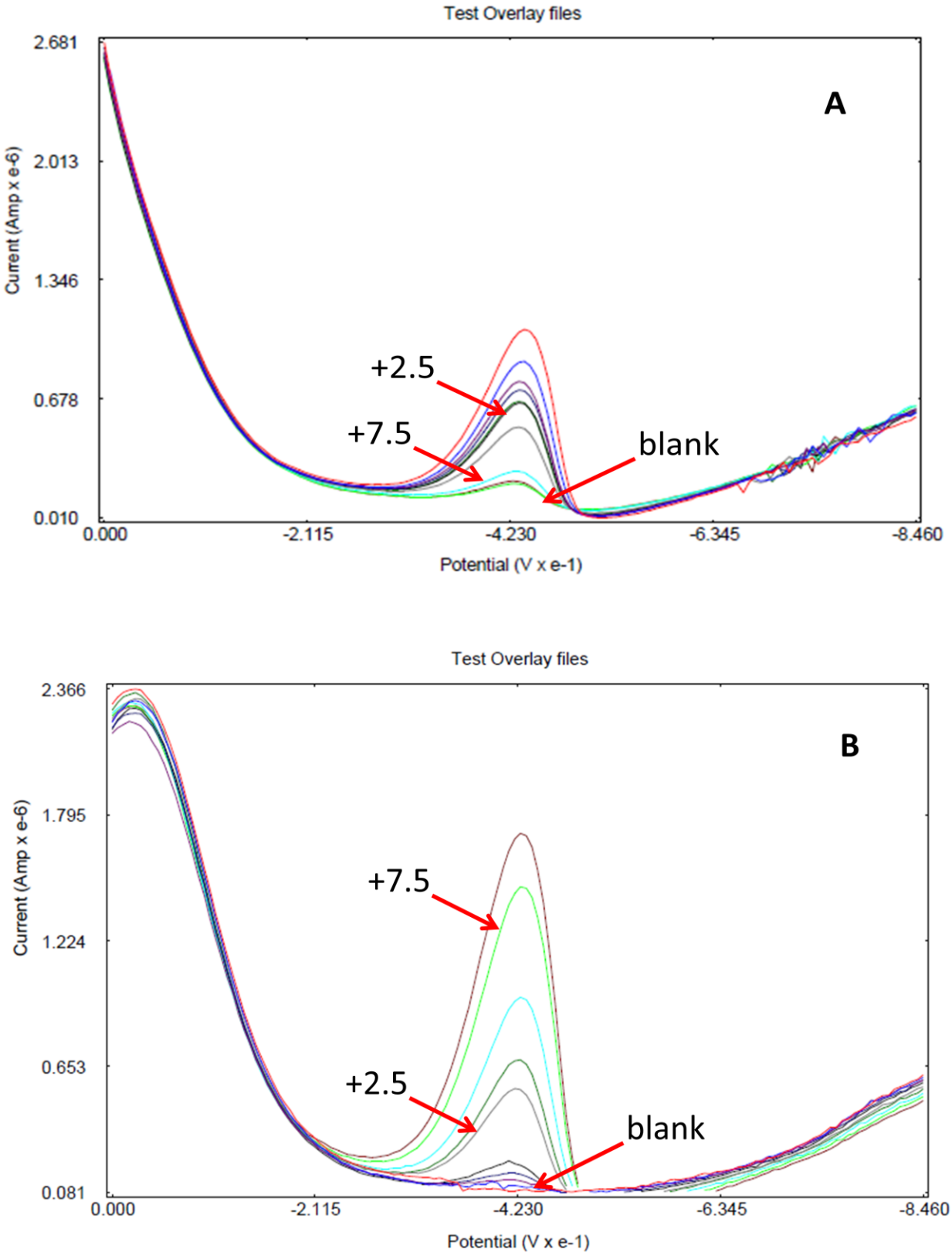

Figure 3 Fe titration overlay. (A) ammonium borate buffer; (B) ultrapure ammonium borate buffer.

4. An exploration of dissolved Fe using Fe-binding ligands

The size fractionation of dissolved iron and organic iron-binding ligands was investigated in the upper ocean of two stations with variable atmospheric dust loadings from the GA03 U.S. GEOTRACES North Atlantic transect. The size fractionation of iron and ligands was measured using cross-flow filtration methods, followed by analysis by isotope dilution inductively-coupled plasma mass spectrometry (ID-ICP-MS) for iron and competitive ligand exchange-adsorptive cathodic stripping voltammetry (CLE-ACSV) for iron-binding ligands. On average, 80% of the dissolved iron (<0.2 μm) was partitioned into the colloidal iron (cFe) pool (10kDa < cFe < 0.2 μm) at all depths and at both stations, as expected for areas of the ocean underlying a dust plume. The organic iron-binding ligands, however, overwhelmingly (75-77%) fell into the soluble size fraction (<10kDa). As a result, modeling the dissolved iron size fractionation at equilibrium with the observed excess ligand distributions did not accurately predict the partitioning into colloidal and soluble pools. This suggests that either a portion of colloidal ligands are missed by current electrochemical methods because they react with iron more slowly than the equilibration time of our CLE-ACSV methods, or part of the observed colloidal iron is actually inorganic in composition and thus cannot be predicted by our model of unbound iron-binding ligands. This potentially contradicts the prevailing view that greater than 99% of the iron in the ocean is organically complexed. Untangling the chemical form of iron in the upper ocean has important implications for surface ocean biogeochemistry and may affect iron uptake by phytoplankton. This work has been submitted to Marine Chemistry for publication (appendix II).

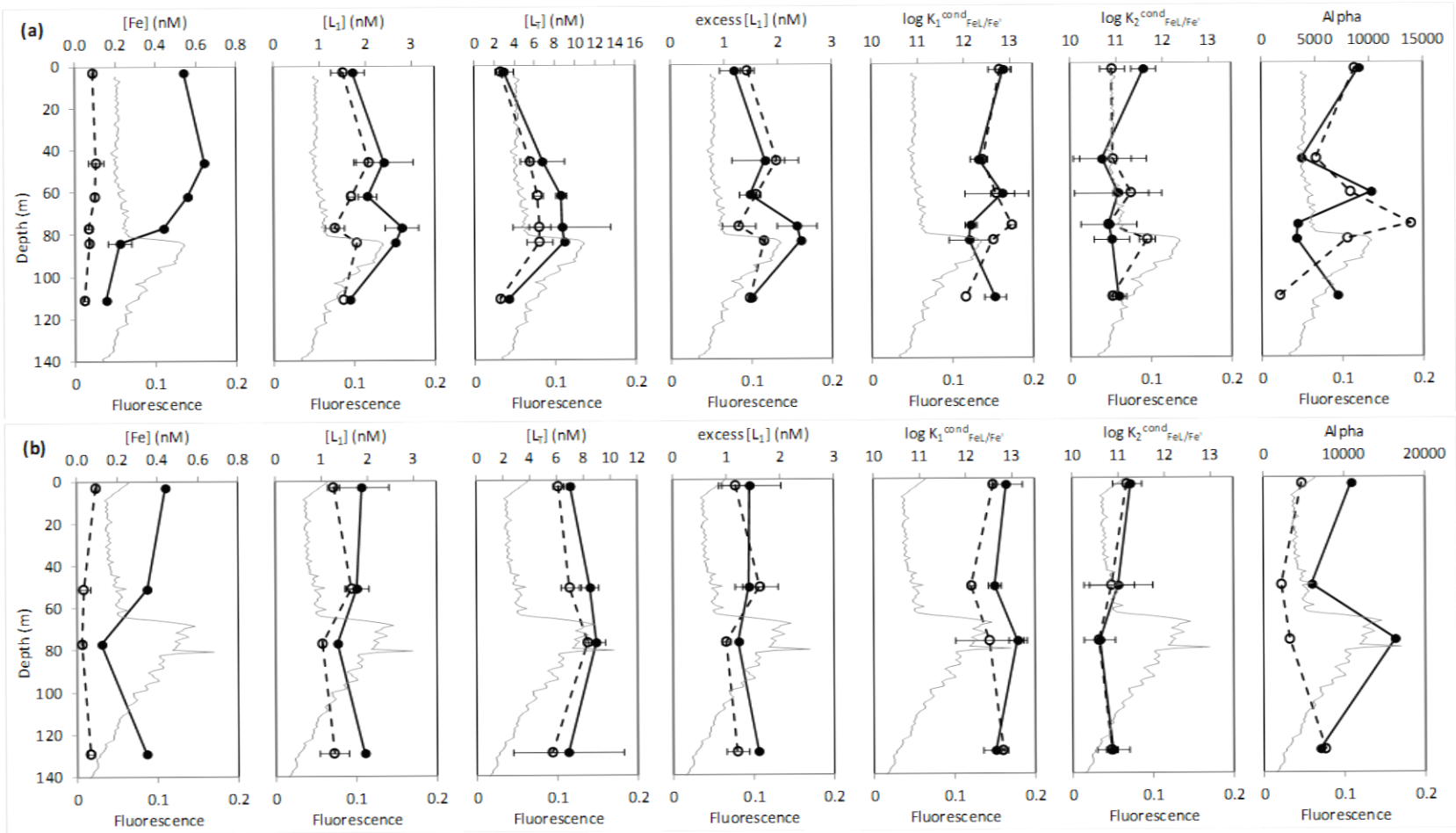

Figure 4. The partitioning of dFe and dissolved Fe-binding ligands in the dissolved (<0.2 µm, solid circles, solid line) and soluble (<10 kDa, open circles, dotted lines) at (a) station 10 (BATS) and (b) station 23 (near Cape Verde). The gray line is the fluorescence trace, and the maximum fluorescence is designated as the deep chlorophyll maximum (DCM). All error bars are ±1 standard deviation.

5. ALOHA temporal variability of Fe-binding ligands

There were two goals for this project: 1. What is the temporal variability of Fe and Fe-binding ligands in the surface ocean on short timescales?

The results of the 13-day time-series from the HOE-PhoR-1 cruise suggest that there is temporal variability. Excess ligand (xs ligands) concentrations ([L]-[Fe]) ranged between 0.4 - 0.93 nM over the 12 days of study (Figure 5), and it roughly appears that excess Fe ligands lag behind variations in Fe by a day. If these ligands are produced biologically in the upper ocean (mixed layer), then this data suggests that it takes ~1 day for these organisms to produce additional ligands.

The second goal to see what is the temporal variability of Fe and Fe-binding ligands with depth at Station ALOHA?

The last time Fe ligands were measured at station ALOHA was in 1994 (Rue and Bruland 1995, Figure 6A). They had relatively low resolution with depth and only one time point of sampling. We have 5 profiles from 2012-2013. Rue and Bruland (1995) detected two ligands through the upper 300m of ALOHA, while we only detected one ligand. Our [L] profiles look like our dFe profiles (Figure 6), as do our excess ligand profiles: surface maximum, with a minimum near or directly below the deep chlorophyll maximum (usually ~130m depth). Oftentimes people see a maximum in ligands at the DCM, and we definitely don't see that at any of our timepoints, not sure why. Perhaps a consequence of which biological populations are living at which depths at ALOHA, since not all organisms produce ligands.

There is definitely temporal variability in ligand concentrations at the surface. The two highest xsLigand concentrations match the dates with the two highest dissolved Fe concentrations, so again it would appear that ligand production is linked to higher dFe concentrations. However at the lower xs ligand concentrations, there is not as clearly a matchup the lowest dFe concentrations do not correspond to the lowest ligand concentrations. Surprisingly, the xsL profile on 7/23/12 stands out much lower than the other profiles (Figure 7). The ligands below ~500m reach were very high concentrations (>2 nM) of excess ligands. Our guess would be that this is might be related to the influence of hydrothermal activity from Loihi near the Big Island of Hawaii. It is certainly consistent with what we saw in the South Pacific, but we still not sure if

it is real. We are at least confident in the 6/2/2013 profile from HP-1 cruise because it is so much higher than the other profiles. Additionally, the dFe hydrothermal contribution in HP-1 was the second lowest I observed in any profile. We are confused why the ligands would be so abundant there if the hydrothermal influence was attenuated. More future investigations are required in order for better understanding of Fe binding ligands profile in the ocean. Manuscript for this study is under preparation for publication.

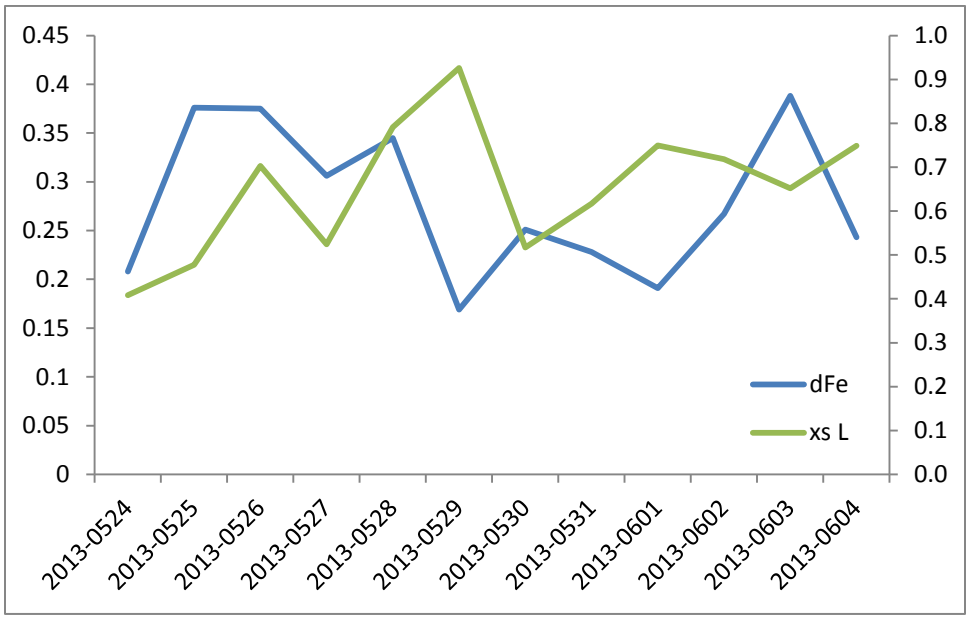

Figure 5 Temporal variability of Fe and Fe-binding ligands in the surface ocean on short timescales

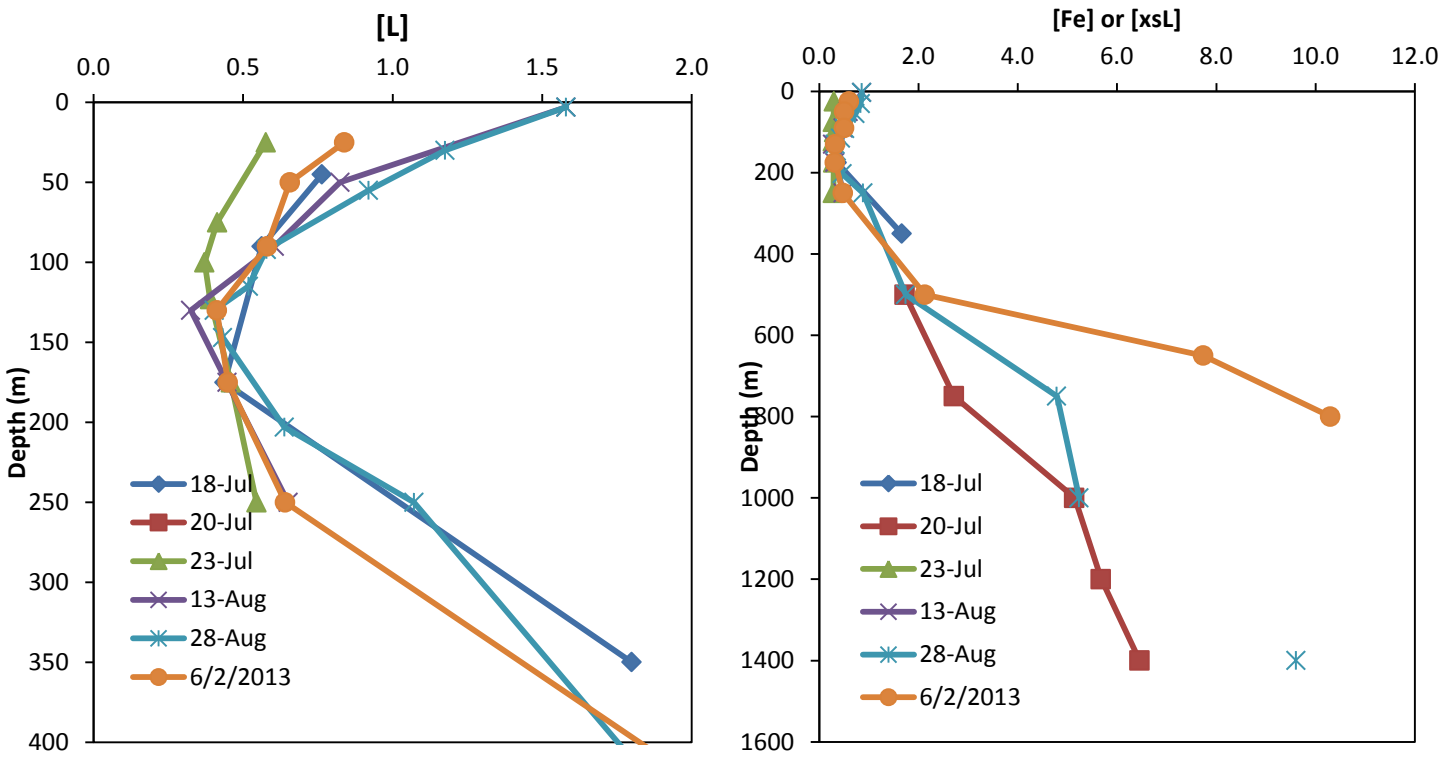

Figure 6 Fe ligands and dFe profiles

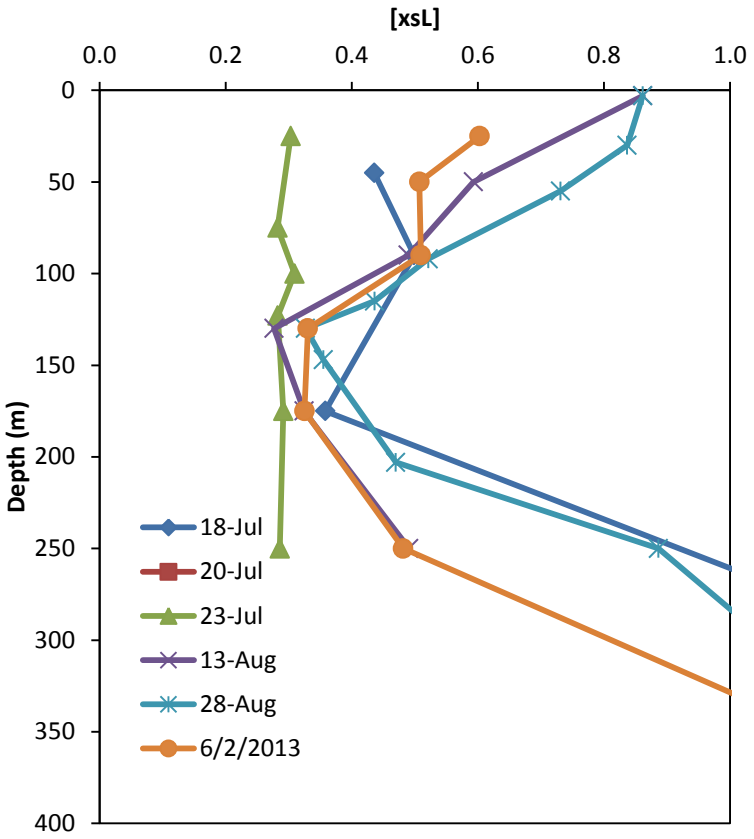

Figure 7 Excess Fe ligands profile

6. References

- Brand, L.E., Sunda, W.G., Guillard, R.R.L., 1986. Reduction of marine phytoplankton reproduction rates by copper and cadmium. Journal of Experimental Marine Biology and Ecology 96, 225-250.
- Bruland, K.W., 1989. Complexation of zinc by natural organic ligands in the central North Pacific. Limnology and Oceanography 34, 269-285.
- Buck, K., Bruland, K.W., 2005. Copper speciation in San Francisco Bay: A novel approach using multiple analytical windows. Marine Chemistry 96, 185-198.
- Buck, 2013. U.S. GEOTRACES North Atlantic: Organic complexation of dissolved Fe. GEOTRACES workshop. Norfolk VA, 2013.
- Buesseler, K.O., S.R. Jayne, N.S. Fisher, I.I. Rypina, H. Baumann, Z. Baumann, C.F. Breier, E.M. Douglass, J. George, A.M. Macdonald, and others, 2012. Fukushima-derived radionuclides in the ocean and biota off Japan. Proceedings of the National Academy of Sciences of the United States of America 109:5,984–5,988.
- Gledhill, M., Mccormack, P., Ussher, S., Achterberg, E.P., Mantoura, R.F.C., and Worsfold, P.J, 2004. Production of siderophore type chelates by mixed bacterioplankton populations in nutrient enriched seawater incubations. Marine Chemistry 88, 75–83.
- Hoffmann, S.R., Shafer, M.M., Armstrong, D.E., 2007. Strong colloidal and dissolved organic ligands binding copper and zinc in rivers. Environmental Science and Technology 41, 6996-7002.
- Hong, S., Boutron, C.F., Barbante, C., Hur, S.D., Lee, K., Gabrielli, P., Capodaglio, G., Ferrari, C.P., Turetta, C., Petit, J.R., Lipenkov, V.Y., 2005. Glacial–interglacial changes in the occurrence of Pb, Cd, Cu and Zn in Vostok Antarctic ice from 240 000 to 410 000 years BP. Journal of Environmental Monitoring 7, 1326-1331.
- Ito, A. and Feng, Y., 2010. Role of dust alkalinity in acid mobilization of iron. Atmospheric Chemistry and Physics, 10: 9237–9250.
- Mawji, M., Gledhill,M., Milton, J.A., Zubkov, M.V., Thompson, A., Wolff, G.A., Achterberg, E.P., 2011. Production of siderophore type chelates in Atlantic Ocean

waters enriched with different carbon and nitrogen sources. Marine Chemistry 124, 90–99.

- Moore, J.K., Doney, S.C., Glover, D.M. and Fung, I.Y., 2002. Iron cycling and nutrient-limitation patterns in surface waters of the World Ocean. Deep Sea Research Part II: Topical Studies in Oceanography, 49(1-3): 463-507.
- Morel, F.M.M., Price, N.M., 2003. The biogeochemical cycles of trace metals in the oceans. Science 300, 944-947.
- Rue, E.L. and Bruland, K.W., 1995. Complexation of iron(III) by natural organic ligands in the Central North Pacific as determined by a new competitive ligand equilibration/adsorptive cathodic stripping voltammetric method. Marine Chemistry, 50(1-4): 117-138.
- Saito, M.A., Moffett, J.W., 2001. Complexation of cobalt by natural organic ligands in the Sargasso Sea as determined by a new high-sensitivity electrochemical cobalt speciation method suitable for open ocean work. Marine Chemistry 75, 49-68.
- Smetacek, V., Klaas, C., Strass, V.H., Assmy, P., Montresor, M., Cisewski, B., Savoye, N., Webb A., d'Ovidio, F., Arrieta, J.M., Bathmann, U., Bellerby, R., and many more, 2012. Deep carbon export from a Southern Ocean iron-fertilized diatom bloom. Nature 487, 313.
- Sunda, W.G., 2013. Feedback interactions between trace metal nutrients and phytoplankton in the ocean. Frontiers in Microbiology DOI: 10.3389/fmicb.2012.00204.
- Velasquez, I., Nunn, B.L., Ibisanmi, E., Goodlet, D.R., Hunter, K.A., and Sander, S.G., 2011. Detection of hydroxamate siderophores in coastal and sub-antarctic waters off the southeastern coast of New Zealand. Marine Chemistry 126, 97–107.

7. Acknowledgment

I would like to thank the following individuals (in no particular order) for facilitating this fellowship opportunity.

- Dr. Murad Abu-Khalaf, Executive Director, Kuwait-MIT Center
- Mr. Khalid Almuhailan, Director, Office of International Programs, KFAS
- Dr. Naji Al-Mutairi, Director General, KISR
- Dr. Adnan Shihab-Eldin, Director General, KFAS
- Prof. Edward Boyle, MIT
- Dr. Jessica Fitzsiommons, MIT/ Rutgers University
- Ms. Laura Guild, Kuwait-MIT Center

The financial support from the Kuwait Foundation for Advancement for Science and the Kuwait Institute for Scientific Research is also acknowledged.

Appendix I

CLE-ACSV method for Fe-binding ligand concentration and strength

1. **Supplies needed to set up ACSV for Fe:**

- Clean lab space (flow bench)
- Ammonium borate buffer: make this by combining 0.4 N ultrapure NH4OH with 1.5M boric acid until the pH is 8.0 (store at room temperature, and keep a "working" bottle of this separate from the stock bottle)
- 5 mM SA (in 100% MeOH) - store this in the refrigerator when not in use, this is good for at least a month at a time, possibly more
- 10+ clean Teflon vials (Savillex) for each titration
- Fe standards diluted in pH 1.8 ultrapure HCl
- BioAnalytical Systems (BAS*i*) Controlled Growth Mercury Electrodes (CGME) set to the Static Mercury Drop setting (drop size “14”)
- BASi E2 electrochemical analyzer
- liquid mercury from Bethlehem company
- glass capillary [BASi]
- Pt electrode [MW-1034; BASi]
- Reference electrode [MF-2052; part BASi]
- Teflon electrochemical cells (trace metal clean) - at least 2 in case one gets dirty
- 2 squirt bottles (one for pH 2 ultrapure HCl, one for clean water)
- small stir bar for electrochemical cell [ER-9132 BASi]
- 3'' Teflon stir bar from VWR
- Micropipets and tips: one 5-10mL, one 100-1000uL, and one 10-100uL adjustable (at least)
- Tip rinse solutions (in 250mL bottles): one 0.06 M ultrapure HCl, one clean water

2. **Electrode setup**

   a. Use the BASi manual to load mercury into the reservoir (including removing air from the reservoir to avoid bubbles)
   b. Plug the CGME into Analyzer, and plug the Analyzer into the laptop (again see the BASi manual for instructions)
   c. Prepare all reagents, as listed above
   d. Condition Teflon vials (at least 1 day before analysis)
      i. 10 ml of Milli-Q were added to 10 acid-cleaned (first clean: concentrated aqua regia, additional cleaning: 3 N HCl and 10x clean water rinsing) Teflon vials (Savillex, 15mL flat bottom)
      ii. 50 µL of the borate-ammonium buffer stock was added to each vial
      iii. Each aliquot was then conditioned with Fe additions of + 0, 0, 0.25, 0.5, 1, 1.5, 2, 2.5, 3.5, 5, 7.5 and 10 nmol L^{-1}
      iv. Note: Conditioning of the vials is *incredibly* important to produce nice titration data! If >10 nM Fe additions will be made in these vials or high Fe samples will be run, condition the vials more appropriately before use!

Fe speciation titrations

1. The frozen (20°C) seawater sample was transferred to the fridge (4°C) 1 day before analysis to let it thaw slowly. In case the sample is not thawed completely the aliquot was microwaved for 3x 10s with 10s cooling period between heating steps.
2. 10 ml of filtered seawater sample was added to the 10 acid-cleaned conditioned vials. Remember to return the sample back to the fridge once you finish this step.
3. Each aliquot was then buffered with a 50 µL addition of the borate-ammonium buffer.
4. Add Fe additions (extra titration point could be added depending on Fe sample concentration) of + 0, 0, 0.25, 0.5, 1, 1.5, 2, 2.5, 3.5, and 5 nmol L^{-1}. Aim to titrate with at least 4x the measured Fe concentration to start.
5. The added Fe was allowed to equilibrate with the natural ligands present in the sample for at least 2 h.
6. 50 µL of 5 mM SA was added to each vial. SA, ambient ligands and Fe were allowed to equilibrate for 15 min before analysis by ACSV.
7. Make ACSV analysis (see settings below).

Fe ACSV settings:

Go to change parameters

- Deposition time: 150 sec (for samples <1000m depth); 300 sec (for samples 1000-1500m depth); 600 sec (for samples >1500m depth)
- Stir rate: 600 rpm
- Quiet period: 15 sec
- Initial potential: 0 mV
- Final potential: -850 mV
- Step potential: 6 mV
- Pulse amplitude: 50 mV
- Pulse width: 35 msec
- Pulse period: 200 msec
- Current full scale: 10 µA
- Filter: 100 Hz
- Scan rate: 20 V/s
- Sample period: Insecond

Starting ACSV

1. Go to EpsilonEC-usb and create a folder (analysis date)→ subfolder for each sample (Cruise -site#-depth)→subfolder metal ligand (i.e. Fe).
2. Go to Experiment tool→change parameters; apply ACSV settings (look above at Fe ACSV settings). In the same tool go to the Setup/Manual Settings (I/O); tick CGME SMDE MODE box.
3. Clean the electrodes properly with pH 2 followed by 2 rinses with dH_2O.
4. Calibrate the ACSV first with test seawater until you get a stable signal. In the cup add 10 ml of test seawater+50 µL boric buffer+50 µL SA; and press run. Clean the electrode with dH_2O at the end of each analysis. Repeat this step 2-3 times until you get a very stable signal with no peak.
5. Start the Fe titration from the lowest Fe concentration (i.e +0 vial) to the highest (i.e. +10 vial). Save the recorded signal in Fe folder as Cruise -depth-Fe-vial# (with no spaces). Make sure that Hg drop is hanging at the end of each analysis before taking off the cup.

6. Discard the sample with Hg drop in the waste Hg beaker (which is located in fume hood). Clean the electrodes and the cup with dH_2O very well before adding the next vial. Remember to wash and fill the empty vial with dH_2O to make it ready for the next titration.
7. At the end of each titration set clean the cup and the electrodes with pH 2 very well followed by 2-3 good rinses with dH_2O.

Exporting data

1. To open new window for Epsilon software Go to start→All Programs→ EpsilonEC-USB folder→Epsilon EC-usb
2. Go to Graph display tool→file overlay→right click select setup→select the sample folder and remember to put it in Differential Pulse Stripping Voltammetry format. Select 0 vial and press New. Then add the rest of the vials by selecting each one and pressing Add icon to have a copy for each one in DPSV.dao.
3. Open ECDSOFT program (from Dario Omanovic's website)→open folder→open vial DPSV.dao file. Click on Baseline→Curve Points. Zoom in and select the points by using set markers (3 points is enough). Press peak icon to get the peak area.

Excel Calculation

1. Fill up each Column with required information such as: SV=vial #, Fe standard concentration, Final Ip= peak area, S=sensitivity, SA concentration.
2. When you choose the slope for sensitivity, try to use the 2-3 points furthest to the right, but choose only points that have a linear slope. Never include the points that are saturating (sometimes the last 1-2 points). If the y-intercept becomes positive in the titration plot, it probably means the slope you have chosen is too low!
3. ALWAYS plot ALL of the points in blue (series one) in the Scatchard and Langmuir plots. You need to be able to see all of the points in order to make a best guess of which points are the relevant ones to use for the slopes.
    a. For Langmuir slope you need to fit the maximum number of the points to get a straight line with a positive slope and intercept.
    b. Scatchard slope choose the points on the left side of the plot to get straight line with negative slope and positive intercept.
4. If you are having trouble generating a Langmuir or Scatchard curve, then you probably have too low of sensitivity and you need to select new points for the sensitivity calculation.

Appendix II

The composition of dissolved iron in the dusty surface ocean: an exploration using size-fractionated iron-binding ligands

Jessica N. Fitzsimmons[*ab], Randelle M. Bundy[c], Sherain N. Al-Subiai[bd], Katherine A. Barbeau[c], Edward A. Boyle[b]

[a] Rutgers University, Marine Biogeochemistry, 71 Dudley Road, New Brunswick, NJ 08901, USA

[b] Massachusetts Institute of Technology/Woods Hole Oceanographic Institution, Chemical Oceanography, 77 Massachusetts Avenue Cambridge, MA 02139, USA

[c] Scripps Institution of Oceanography, University of California San Diego Geosciences Research Division, 9500 Gilman Drive La Jolla, CA 92093, USA

[d] Environment Management Program, Environment and Life Sciences Research Center, Kuwait Institute for Scientific Research, Kuwait.

[*]Corresponding author:

Jessica Fitzsimmons

Rutgers University

Institute of Marine and Coastal Science

71 Dudley Road

New Brunswick, NJ 08901

Email: jessfitz@marine.rutgers.edu

Highlights

- Mostly soluble (<10 kDa) Fe ligands do not predict colloidal Fe (10kDa-0.2µm) excess
- This could suggest that some colloidal Fe in subtropical N. Atlantic is inorganic
- Or some colloidal ligands are kinetically hindered and thus undetected by CLE-ACSV

Keywords

iron

iron ligands

CLE-ACSV

colloids

ultrafiltration

trace metals

GEOTRACES

North Atlantic Ocean

chemical oceanography

Abbreviations

cFe- colloidal iron (10kDa < cFe < 0.2 μm)

CLE-ACSV- competitive ligand exchange adsorptive cathodic stripping voltammetry

CFF- cross flow filtration

dFe- dissolved iron (< 0.2 μm)

Fe- iron

ID-ICP-MS- isotope dilution inductively-coupled plasma mass spectrometry

sFe- soluble iron (< 10kDa)

Abstract

The size fractionation of dissolved iron and organic iron-binding ligands was investigated in the upper ocean of two stations with variable atmospheric dust loadings from the GA03 U.S. GEOTRACES North Atlantic transect. The size fractionation of iron and ligands was measured using cross-flow filtration methods, followed by analysis by isotope dilution inductively-coupled plasma mass spectrometry (ID-ICP-MS) for iron and competitive ligand exchange-adsorptive cathodic stripping voltammetry (CLE-ACSV) for iron-binding ligands. On average, 80% of the dissolved iron (<0.2 μm) was partitioned into the colloidal iron (cFe) pool (10kDa < cFe < 0.2 μm) at all depths and at both stations, as expected for areas of the ocean underlying a dust plume. The organic iron-binding ligands, however, overwhelmingly (75-77%) fell into the soluble size fraction (<10kDa). As a result, modeling the dissolved iron size fractionation at equilibrium with the observed ligand distributions did not accurately predict the partitioning into colloidal and soluble pools. This suggests that either a portion of colloidal ligands are missed by current electrochemical methods because they react with iron more slowly than the equilibration time of our CLE-ACSV methods, or part of the observed colloidal iron is actually inorganic in composition and thus cannot be predicted by our model of unbound iron-binding ligands. This potentially contradicts the prevailing view that greater than 99% of dissolved iron in the ocean is organically complexed. Untangling the chemical form of iron in the upper ocean has important implications for surface ocean biogeochemistry and may affect iron uptake by phytoplankton.

1. Introduction

Since iron (Fe) is known to limit primary production in large portions of the global ocean (Moore et al., 2002), much of the exploration of marine dFe biogeochemistry involves attempts to link Fe fluxes in the surface ocean with the biological uptake of dissolved Fe by microorganisms. The biological utilization of Fe during photosynthesis, nitrogen fixation, and remineralization (Morel et al., 2003; Sunda, 2012) is what ties Fe biogeochemistry to the global carbon cycle and ultimately climate. However the transfer efficiency of "new" dissolved Fe from lithogenic source to biologically available form (currently believed to be Fe(II); Morel et al., 2008; Shaked et al., 2005) is ultimately controlled by the changing chemical composition of Fe along this elusive transformation pathway, since processes such as scavenging/precipitation, Fe exchange, and photochemistry can alter the speciation and thus the reactivity and fate of each Fe species along the way.

Much has been learned about the composition of dFe over the last several decades. Dissolved Fe (dFe, here defined as <0.2 μm) has a broad size distribution comprised of both "truly dissolved" soluble Fe (sFe <10kDa) and "small particulate" colloidal Fe (10kDa < cFe < 0.2 μm) size fractions (Bergquist et al., 2007; Chever et al., 2010; Fitzsimmons and Boyle, in review; Nishioka et al., 2001; Ussher et al., 2010; Wu et al., 2001). Incubation studies have shown that while a limited number of cFe forms are highly bioavailable (such as exopolymeric saccharides, Hassler et al., 2011b), sFe is typically preferred and is taken up into the cell much faster than cFe (Chen et al., 2003; Chen and Wang, 2001; Wang and Dei, 2003), and inorganically complexed cFe (such as nanoparticulate Fe oxyhydroxides) is not directly available at all (Rich and Morel, 1990). In addition, studies using competitive ligand exchange electrochemical measurements have suggested that >99.9% of marine dFe is bound by organic

ligands (Rue and Bruland, 1995; van den Berg, 1995; Wu and Luther, 1995) that maintain marine dFe above its ~0.1 nM inorganic solubility in pH 8 seawater (Liu and Millero, 2002; Millero, 1998). While a few of these organic ligands have been identified as hydroxamate siderophores (Mawji et al., 2011; Velasquez et al., 2011; Vraspir and Butler, 2009), chemically characterized ligands only comprise a small percentage of the total dFe pool. In general, the identity of marine Fe-binding ligands is largely unknown (Gledhill and Buck, 2012).

However, the hypothesis that nearly all marine dFe is organically bound relies on an assumption of thermodynamic equilibrium between dFe and dissolved Fe-binding ligands in the open ocean. Additionally, electrochemical characterization of Fe-binding ligands is somewhat limited, as only the Fe-binding ligands that are kinetically labile over the period of equilibrium with the added ligand can be detected, causing any refractory forms of dFe to be measured as a very strong ligand. Despite these shortcomings with electrochemistry, hardly any studies specifically measuring the chemical binding environment of dFe have been completed, largely because of analytical obstacles. One analysis of colloidal Fe composition by energy dispersive spectroscopy showed that open ocean cFe is mostly organically bound (Wells and Goldberg, 1992), while in contrast a recent study using synchrotron technology demonstrated that a portion of the surface colloidal Fe underlying dust plumes in the Southern Ocean is inorganic, composed of tiny bits of magnetite (von der Heyden et al., 2012). Thus, while a long-standing assumption regarding the chemical composition of marine dFe is that the overwhelming majority is bound by strong organic Fe-binding ligands, there is a possibility that some dFe, especially in the colloidal phase, is inorganically bound (nanoparticulate). This might be especially true in regions where continental Fe sources are known to be significant, such as underlying dust plumes,

downstream of hydrothermal vents, near the continental margin, in regions with abundant glacial meltwater, *etc.* (Fitzsimmons et al., in review).

The chemical composition of dFe has the greatest influence on productivity in the upper ocean where phytoplankton are most active, and simultaneously the surface ocean is the region where atmospheric dust deposition occurs, arguably the most significant Fe input to the ocean (Jickells et al., 2005; Mahowald et al., 2005). The solubility of aerosol Fe is variable and depends on a suite of factors including aerosol composition, source (anthropogenic or crustal), and size, as well as seawater pH and Fe-binding ligand concentration (Baker and Croot, 2010). Studies of the size partitioning of dFe have consistently shown that in the surface ocean underlying dust plumes, dFe is preferentially maintained in the colloidal size fraction (Bergquist et al., 2007; Fitzsimmons and Boyle, 2014b; Fitzsimmons et al., in review; Ussher et al., 2010; Wu et al., 2001), while in the surface ocean of low-dust regions, the smaller soluble size fraction dominates the dFe pool (Boye et al., 2010; Chever et al., 2010; Nishioka et al., 2003; Wells, 2003). Colloidal Fe has also been shown to be the dominant Fe size fraction yielded in seawater leaches of natural dust (Aguilar-Islas and Mehalek, 2013; Aguilar-Islas et al., 2010).

This raises two important questions: what is the binding environment of dFe in the surface ocean after recent dust deposition, and how much of this dust-derived dFe is bioavailable? It is possible for the dust-derived surface maximum in cFe to assume any of three possible compositions: Fe bound by colloidal-sized organic ligands after solubilization from dust, colloidal-sized bits of dust that physically separated from the dust particles upon impacting the surface ocean (resulting in a nanoparticulate cFe composition of the same composition as the dust), or Fe that was initially solubilized from dust in the surface ocean but then re-precipitated *in situ* and aggregated to colloidal size (also resulting in a nanoparticulate cFe composition,

presumably amorphous Fe oxyhydroxides). Which of these three forms comprises the majority of surface dFe underlying dust plumes would have a significant influence on the residence time and bioavailability of surface dFe pools, and thus the distinction between these is at the crux of the problem linking dust deposition to biological uptake of dFe.

In this paper, we explore the binding environment of dFe in the surface of the high-dust North Atlantic Ocean using an analysis of the Fe-binding ligand concentration and strength of both the soluble and dissolved Fe pools. We aim to consider whether there could be a natural inorganic component to the colloidal Fe pool of the surface ocean, which would provide an exception to the prevailing view that >99.9% of dFe is believed to be bound by organic ligands.

2. Methods

2.1 Sample collection

Seawater samples for this study were collected from two stations on the U.S. GEOTRACES GA03 North Atlantic Zonal Transect 2011 cruise (Nov-Dec 2011): Station 10 at 31.933°N, -64.733°W near the Bermuda Atlantic Time Series (BATS) site and Station 23 at 18.39°N, -26.765°W near the Cape Verde Islands (Figure 1). Trace metal uncontaminated seawater was collected using the U.S. GEOTRACES GO-FLO rosette by the methods described in Cutter and Bruland (2012). GO-FLO bottles were carried individually into an ISO 5-rated clean van, where the seawater was filtered through pre-cleaned 0.2 µm Pall Acropak-200™ Supor® capsule filters under ~0.4 atm of HEPA-filtered air. Surface samples were collected using the GeoFish system of the Bruland lab, which employs all-PFA tubing attached to a vane that coasted at ~3 m depth suspended from a boom off the starboard side of the ship during

forward ship motion at up to 12 knots. An all-PFA diaphragm pump sipped clean seawater through this system at ~0.5 atm pressure, and filtration was completed first through a 0.45 µm Osmonics (PFA) filter and then through a 0.2 µm polycarbonate track etched filter mesh held in a polypropylene housing. Filtrates were taken into acid cleaned 4L LDPE bottles after three bottle rinses. Sub-samples of this 4L were taken into 30 mL HDPE bottles for Fe concentration analysis and into 500 mL fluorinated polyethylene (FLPE) bottles for the dFe-binding ligand analysis. FLPE bottles had been conditioned with ultra clean MilliQ water for more than a month before sample collection to remove all acid residue. To collect the sFe fraction (< 10 kDa), the rest of the 4L filtrates were immediately filtered again through an all-Teflon cross-flow filtration (CFF) system in static mode (Fitzsimmons and Boyle, 2014a). A Millipore Pellicon XL (PLCGC) 10 kDa regenerated cellulose CFF membrane was employed, and 300-350 mL of sample seawater was first flushed through the system to condition the membrane and CFF tubing against Fe sorption, after which the permeate stream was collected as the sFe or sFe-ligand sample. After filtration and ultrafiltration, Fe-binding ligand samples were frozen un-acidified until analysis, and Fe concentration samples were acidified to pH 2 using 6N hydrochloric acid that had been distilled four times in a Vycor still (Fe concentration ~ 0.1 nmol/kg).

Additional seawater for analysis of the mass balance of Fe-binding ligands through the CFF system (see section 2.4 below) was collected from the surface Pacific Ocean at 22.75°N, 158°W (Station ALOHA) on 19 July 2013 on the HOE-PhoR-II cruise supported by the Center for Microbial Oceanography: Research and Education. Seawater was pumped from 15 m depth through an all-PTFE diaphragm pump through acid-cleaned tubing into a 0.2 µm Acropak-200 filter and then into acid-cleaned 8L LDPE bottles. Subsamples were collected for dFe (<0.2 µm)

and ultrafiltered for sFe (<10 kDa) concentration and dFe-binding ligand analysis and preserved as described above for the GA03 cruise.

2.2 Fe analyses

dFe and sFe samples were analyzed in triplicate for their Fe concentration at MIT by isotope dilution inductively-coupled plasma mass spectrometry (ID-ICP-MS) on a hexapole collision cell IsoProbe multi-collector ICP-MS. The ID-ICP-MS method employs a ^{54}Fe-spike and batch pre-concentration with nitrilotriacetate resin (Lee et al., 2011). cFe was calculated as the difference between dFe and sFe. Fe procedural blanks using this analytical method averaged 0.044 nmol/kg with a typical standard deviation over a single day's analysis of 0.009 nmol/kg; thus, the reported detection limit was 0.027 nmol/kg. Comprehensive lab analyses of the SAFe S seawater for dFe during the period of these analyses averaged 0.101±0.009 nmol/kg (Bottles 17 and 318, n=6), which agrees well with the consensus value of 0.093±0.008 nmol/kg. Similarly, SAFe D2 standard for dFe during the period of these analyses averaged 0.911±0.018 nmol/kg (Bottle 446, ±1SD, n=15), which also agree well with the consensus value of 0.933±0.032 nmol/kg. Consensus values cited here were updated in May 2013 (www.geotraces.org/science/intercalibration).

2.3 Fe-binding ligand analyses

Measurements of dFe and sFe-binding ligand concentrations and binding strengths were made by competitive ligand exchange-adsorptive cathodic stripping voltammetry (CLE-ACSV)

on a BioAnalytical Systems (BAS*i*) Controlled Growth Mercury Electrode coupled to a BAS*i* Epsilon ε2 voltammetric analyzer by the methods described in Buck et al. (2007). Briefly, 10 mL sample aliquots were buffered to pH 8.2 (NBS scale) with a borate-ammonium buffer in PFA vials (Savillex) that had been previously conditioned to the anticipated Fe addition. Titration Fe additions were made at concentrations ranging from 0-7.5 nM and were allowed to equilibrate for 2 hours before the addition of the added ligand, salicylaldoxime (SA), at concentrations of 25 or 32.3 µM ($\alpha_{Fe(SA)_2}$ = 60 or 100). After a 15 minute equilibration with SA, samples were adsorbed to the mercury drop at zero potential for 2-5 minutes and then stripped at 0.03 V/s using differential pulse mode to a final potential of -0.85 V. Raw titration data were interpreted for their Fe-binding ligand concentration ([L]) and ligand conditional stability constants ($K^{cond}_{FeL,Fe'}$) using the van den Berg/Ružić (Ružić, 1982; van den Berg, 1982) and the Scatchard (Mantoura and Riley, 1975; Scatchard, 1949) linearization techniques, the results of which were averaged to obtain the reported values and error estimates. Sensitivities were determined by internal calibration at the end of the titration, when all ligands are titrated. An $\alpha_{Fe'}$ of 10^{10} was assumed in the Fe speciation calculations.

2.4 Fe-ligand mass balance determination

The mass balance of Fe-binding ligands following CFF was determined on the 15 m Station ALOHA seawater in order to assess the potential loss of ligands during this ultrafiltration, since an ~25-30% loss of dFe has been observed using the same system (Fitzsimmons and Boyle, 2014a). Station ALOHA samples for Fe concentration and Fe-binding ligand concentration and strength were collected and analyzed from the dissolved (< 0.2 µm),

CFF permeate (assumed to be sFe), and CFF retentate (containing some sFe and some cFe) streams. With the permeate and retentate flow rates calibrated identically at 12.5 mL/min each, the concentration factor (CF) in static mode was calculated to be 2.0 using the following equation:

$$CF = \frac{\text{initial sample volume}}{\text{final retentate volume}} = \frac{\text{permeate volume + retentate volume}}{\text{retentate volume}} \quad (1)$$

Under ideal permeation conditions where the membrane does not preferentially retain any soluble compounds (permeation coefficient = 1, Schlosser and Croot 2008), the permeate solution should reveal the sFe and the sFe-binding ligand concentrations (<10 kDa). However, in solutions containing cFe, the Fe and Fe ligand concentrations in the retentate solution must be corrected for the presence of sFe and the degree of CFF concentration in order to calculate the true cFe and cFe-ligand concentrations, as follows:

$$cFe = \frac{[Fe]_{retentate} - [Fe]_{permeate}}{CF} \quad (2)$$

where [Fe] is the concentration of Fe or the concentration of Fe-binding ligands in each fraction. To determine Fe mass balance, the sFe (permeate) and cFe (Equation 2) concentrations were compared to the dFe (< 0.2 µm solution originally fed into the CFF system) concentration, and the same was completed for the total ligand concentration.

3. Results

Large volume seawater samples containing the dissolved (<0.2 µm) and soluble (<10 kDa) Fe size fractions were collected in two regions of the North Atlantic Ocean (Figure 1): the high North African dust flux OMZ region near the Cape Verde Islands (Station 23) and the low

marine dust flux subtropical gyre region near Bermuda (Station 10). These locations were chosen for two reasons. First, we wanted to sample variable dust loading/composition in the surface ocean: Station 10 near Bermuda had 1-2 ng/m^3 Fe loadings with a "marine/North American" source (calculated using HYSPLIT back trajectories, Figure S1) and an Fe solubility of ~7% (in instantaneous water leachate), while Station 23 near Cape Verde had much higher total aerosol Fe loadings >1000 ng/m^3 Fe with a "North African" source and a lower Fe solubility of ~0.4% (solubilities reported from Shelley et al., in review).

Second, we wanted to sample upper ocean regions with variable biogeochemistry and water mass structure (Figure 2 and S2). Station 10 receives influences from the Gulf Stream southern recirculation in the mixed layer (Talley et al., 2011), which extended to 88 m depth (Figure 2a), and then from Eighteen Degree Water (θ=18°C, salinity=36.5, O_2=200 µmol/kg; Worthington, 1959) extending from the bottom of the mixed layer to below 200 m depth. In contrast, station 23 is located where the Canary Current transitions into the North Equatorial current (Talley et al., 2011), bringing waters from the northeast to the southwest. This surface current extended through the mixed layer at 63m (Figure 2b), below which an influence of the salty Subtropical Underwater (STUW: θ=25°C, salinity>37) dominated through 95 m depth. Below ~100 m depth North Atlantic Central Water (NACW) dominated all the way through ~600 m depth. From Figure 2 it is clear that station 10 was situated more in the subtropical gyre with a depressed pycnocline to >350 m depth, while station 23 was situated south of the gyre, with a much shallower pycnocline starting at ~100 m depth, and received influences of oxygen minimum zone (OMZ) waters below ~250 m depth.

This paper will focus on results from size-fractionated soluble and dissolved Fe-binding ligand samples collected in the North Atlantic. For perspective on the Fe biogeochemistry

occurring in the North Atlantic during the time of the GA03 cruise, please see Hatta et al. (in review) for general dFe biogeochemistry, Conway and John (in press) for quantification of Fe sources, Fitzsimmons et al. (in review) for a discussion of the dFe size partitioning into soluble and colloidal phases, Shelley et al. (in review) for marine aerosol Fe fluxes and solubility, and Buck et al. (in review) for the distribution of organic Fe-binding ligand concentrations and strengths.

3.1 Size partitioning of dissolved Fe and Fe-binding ligands

We evaluated the size-partitioning of dissolved Fe and Fe-binding ligands in the upper 150m of the North Atlantic Ocean in order to explore the chemical composition of dust-derived dFe phases. As shown in Figure 3, dFe concentrations were elevated (<0.4 nM) in the surface ocean of both stations, and dFe was ~80% partitioned into the colloidal size fraction (10kDa < cFe < 0.2μm). This surface dominance of dFe by colloidal-sized species was consistent across the entire GA03 North Atlantic transect (Fitzsimmons et al., in review) and was used as evidence that aerosol-derived Fe is preferentially maintained in the colloidal size fraction. This is consistent with other studies demonstrating that in regions where atmospheric dust input is significant, surface dFe is largely maintained in the cFe pool (Bergquist et al., 2007; Fitzsimmons and Boyle, 2014b; Wu et al., 2001). Below the surface at the 70-90m deep chlorophyll maximum (DCM) cFe decreased to a minimum concentration, another feature typical of North Atlantic dFe size partitioning (Fitzsimmons et al., in review)

Organic Fe-binding ligands, however, were overwhelmingly partitioned into the soluble size fraction (Figure 3, Table 1 and 2). Fe ligand concentrations in both pools exceeded the Fe

concentrations in each pool, and thus most of the Fe ligand concentrations reported are free ligands. Two ligand pools were detected at each of the depths measured (L_1 is the stronger ligand class, and L_2 is weaker). At the lower analytical window, both ligand classes were preferentially partitioned into the soluble phase: soluble L_1 ligands averaged 77±17% of the L_1 ligands at station 10 and 75±13% of the L_1 ligands at station 23, and total soluble ligands averaged 78±7% of the total ligands at station 10 and 86±5% of the total ligands at station 23. At the higher analytical window, the pattern of soluble ligand dominance was the same: soluble L_1 ligands comprised 77±12% and 93±7% of the total L_1 ligands detected at stations 10 and 23, respectively. Only at the DCM of station 10 did colloidal ligands comprise the greatest portion of total dissolved ligands (Figure 3), but this pattern was not reproducible at the DCM of station 23.

The $K'^{cond}_{FeL,Fe}$ values for the two ligand classes had variable size partitioning patterns both within a single station and across the two stations (Figure 3). At station 10, log $K'^{cond}_{FeL,Fe}$ values were not significantly different between the two size fractions, except near the DCM where log K_1 was greater at ~13 for the soluble size fraction and nearer to ~12 for the total dissolved size fraction, indicating that colloidal ligands were weaker at this depth. At station 23, log K_2 values were identical between the two size fractions, while log K_1 values were slightly higher in the colloidal fraction than in the soluble fraction at most depths.

Using this size partitioned Fe-ligand binding strength and concentration data together, we determined the capacity for the free Fe-binding ligands in each size fraction to bind Fe, $\alpha_{FeL'}$

$$\alpha_{FeL'} = 1 + ([eL_1] * K_1) + ([L_2] * K_2) \quad (3)$$

where the concentration of excess $[L_1]$ ($[eL_1]$) is the L_1 not bound to Fe:

$$[eL_1] = [L_1] - [Fe] \quad (4)$$

This $\alpha_{FeL'}$ was calculated for each size fraction and is shown in Figure 3. The total dissolved $\alpha_{FeL'}$ was greater than the soluble $\alpha_{FeL'}$ at most depths of station 23, indicating that the colloidal ligands had at least some capacity to bind Fe. Only at the deepest (129 m) depth of station 23 was the dissolved $\alpha_{FeL'}$ the same as the soluble $\alpha_{FeL'}$, indicating that the colloidal ligands had no capacity to bind new Fe at this depth. At the DCM of station 10, in contrast, the soluble $\alpha_{FeL'}$ was greater than the dissolved $\alpha_{FeL'}$, which was related to the greater $\log K^{cond}_{FeL,Fe'}$ values calculated for the soluble ligands than the total dissolved ligands at these depths (Table 3).

The primary objective of this study, however, was to determine whether the size partitioning of organic Fe-binding ligands in the upper ocean would predict the observed size partitioning of dFe. Thus, following Cullen *et al*. (2006), we modeled the fraction of total dFe expected to exist in the soluble phase at equilibrium with the observed size fractionated ligands:

$$\frac{Fe_{sol}}{Fe_{diss}} = \frac{(\alpha_{FeL'})_{sol}}{(\alpha_{FeL'})_{diss}} = \frac{[(K_1*[eL_1])+(K_2*[L_2])]_{sol}}{[(K_1*[eL_1])+(K_2*[L_2])]_{diss}} \quad (5)$$

If dFe is organically bound to ligands with the same concentration and strength as calculated using the $\alpha_{FeL'}$value of the observed free ligands, then the modeled partitioning should match the observed dFe partitioning (in this case, the left-most and the right-most panels of Figure 3 should match).

We also compared the modeled and observed soluble Fe partitioning fractions in Figure 4, and the observed sFe fractions all fell below the modeled-observed 1:1 line, indicating that the size partitioning of organic ligands as measured by electrochemistry does not predict the observed dFe size partitioning in the upper ocean of either station.

3.2 Mass-balance of Fe-binding ligands using CFF

It is well known that Fe recovery during CFF can be low (Reitmeyer et al., 1996), and using the same low-surface area, regenerated cellulose cross flow filtration system as in this study, Fitzsimmons and Boyle (2014a) lost 25-30% of the dFe they originally put into the CFF system to the surface and/or pores of the CFF filter. They used various lines of evidence to posit that it was only the colloidal fraction that was lost/trapped in the filter membrane, while sFe was fully recovered in the permeate solution. It was important to prove that this was also true for the free and bound Fe-binding ligand fractions in order for the calculations of this study to be robust.

Thus, at Station ALOHA (22.75°N, 158°W) in the Pacific Ocean, the mass balance of Fe-binding ligands during CFF was determined at 15 m depth (Table 4). Fe concentration and Fe-binding ligand concentration and strength were measured for the permeate, retentate, and initial CFF feed solutions. The soluble Fe and Fe-binding ligand concentrations were assumed to be equal to that found in the permeate (ideal permeation characteristics of the CFF membrane were assumed here, as they were determined for Fe concentrations in Fitzsimmons and Boyle, 2014a), and the initial CFF feed solution was set equal to the "dissolved" <0.2 µm fraction. Colloidal Fe and ligand concentrations derived from the CFF system were calculated using Equations 1-2. Using the definitions of soluble and colloidal sizes, soluble Fe (defined here as <10 kDa) plus colloidal Fe (defined here as between 10 kDa and 0.2 µm) should equal dissolved Fe (defined as < 0.2 µm). Thus, the measured "soluble+colloidal" concentration was compared to the measured dissolved concentration in the CFF feed solution to determine the mass balance:

$$\%\ \text{Recovery} = \frac{[\text{Soluble}]_{\text{meas}} + [\text{Colloidal}]_{\text{meas}}}{[\text{Feed solution}]_{\text{meas}}} * 100\% \qquad (6)$$

These calculations were completed for the Fe concentration, the total ligand concentration, and the excess ligand concentration (Table 4). The Fe recovery from the CFF system was low at 54±27%, which is within error of the average 70-75% mass balance for Fe concentration recorded using the same system by Fitzsimmons and Boyle (2014a) across several sampling sites in the Pacific and Atlantic Oceans. The large 27% error is attributed to the extremely low concentrations of sFe (0.039±0.008) measured at this station. The total ligand recovery was quite similar at 65±27%, and when only the excess ligand is considered, the recovery was 69±34%. Since the recoveries were so similar between Fe and L concentrations, we can safely assume that the same mechanism that causes cFe loss to the CFF membrane, which Fitzsimmons and Boyle (2014a) attributed to either cFe accumulation on the CFF membrane or cFe entrapment in the pores of the CFF membrane, also causes free colloidal ligand losses to the CFF membrane. Free soluble ligands, in contrast, likely permeate the membrane completely. While we cannot prove this conclusively as Fitzsimmons and Boyle (2014a) did for deep Atlantic sFe, the fact that the soluble ligand fraction accounted for the majority of the dissolved ligand pool supports the conclusion that the majority of soluble ligands are recovered by CFF. This indicates that the size partitioning conclusions drawn in this study using the dissolved and soluble (permeate) ligand measurements are valid; only retentate ligand measurements are affected by poor recovery and should be avoided. Colloidal ligand concentrations can thus be calculated using the following equation (instead of Equation 2):

$$[\text{colloidal L}] = [\text{dissolved L}] - [\text{soluble L}] \quad (7)$$

4. Discussion

The data presented here demonstrates that the size partitioning of Fe ligands into soluble and colloidal fractions is variable with depth and location, with a dominance of soluble ligands in the excess ligand pool. Similar results were also observed in the upper 200m by Boye *et al.* (2010) in the Southern Ocean (200 kDa filter used), by Thuroczy *et al*. (2010) in the Northeast Atlantic Ocean (1000 kDa filter used), and by Cullen *et al*. (2006) in the North and South Atlantic Oceans (0.02 µm filter used).

With these results, we aimed to explore the chemical composition of the colloidal Fe maximum found in surface ocean regions underlying dust plumes, particularly whether it is organically or inorganically bound. We based our interpretation of these size fractionated ligand results on the hypothesis that if the size partitioning of free surface Fe-binding ligands into soluble and colloidal fractions predicted the observed surface dFe size partitioning, then surface dFe is likely bound by organic ligands. It is clear from the results of Figures 3 and 4 that this was not the case: observed free Fe-binding ligands were primarily soluble, while observed dFe was mostly colloidal in size. This does not preclude an organic composition of the colloidal Fe in the dusty surface North Atlantic. However, it must mean that either (1) we are missing a fraction of free colloidal ligands in our electrochemical measurements, or (2) some portion of the cFe in the surface ocean is inorganic in composition (not controlled by equilibrium with a size-partitioned set of free organic ligands, as our calculations assume).

To evaluate these possibilities, we must consider the assumptions involved in the electrochemical measurements of Fe binding ligands and the α_{FeL}, calculations (Equation 5, Figure 4) used in this study. First, CLE-ACSV can only detect ligands that are able to exchange with Fe on the timescale of the analytical equilibrium (in this case, 2 hours with added Fe and 15 minutes with SA). Thus, any kinetically-inhibited ligands would not be detected by this CLE-

ACSV method, and our measured ligand concentrations could be underestimates. Some other CLE-ACSV methods use longer equilibration times (8-12 hours) with the added ligand (e.g., Gledhill and van den Berg, 1994) because the Fe and the added ligand are not introduced sequentially, such as was done in this study. This ensures that the natural ligands and the added ligand are in equilibrium with the added metal before analysis, which can take longer when the Fe′ is decreased by the added ligand. However, one advantage of these methods is that the longer equilibration times may allow for the detection of additional ligands (likely weaker ligands), which could have more sluggish kinetics.

We aimed to estimate what concentration of "kinetically-inhibited" colloidal-sized free ligands would be required to predict the observed dFe size partitioning. The majority of known colloidal Fe-binding ligands in the marine environment fall into the weaker (L_2) ligand class, such as polysaccharides (Hassler et al., 2011a), , and humic-like substances (Laglera and van den Berg, 2009). Thus, for the purposes of these preliminary calculations we assumed any missing colloidal ligands had the binding strength of the L_2 colloidal ligands we measured, which we calculated for both L_1 and L_2:

$$[L]_{diss}K_{diss} = [L]_{sol}K_{sol} + [L]_{coll}K_{coll} \quad (8)$$

The colloidal ligand concentrations (calculated using Equation 7) and binding strengths (Equation 8) are tabulated in Table 5. In a few cases we were not able to calculate a K_{coll} within the errors of our measurements.

Using these estimates, we calculated the concentration of "kinetically inhibited" colloidal-sized ligands at the colloidal K_2 strength that would be required to predict the observed dFe size partitioning (Table 5). The "missing colloidal ligand" concentrations at station 23

ranged from 0.03-7.63 nM, while the concentrations at station 10 were incalculable or reached very high concentrations that are not oceanographically consistent. Notably, the lowest concentrations of "missing colloidal ligands" were calculated at or right below the DCM. This makes sense because it is at these depths that more of the dFe was soluble .

These missing ligands would need to be unbound colloidal-sized ligands that bind dFe in the ocean with kinetics more sluggish than the 2 hour equilibration time of our CLE-ACSV measurement. Our assumption that these ligands have a binding strength of the measured colloidal K_2 is the weakest assumption in our calculation; if the ligands were significantly weaker than assumed, our calculated missing colloidal [L] concentrations would be underestimates. Another possibility, however, is that a high concentration of a colloidal ligand is reflected in the electrochemical data as a very strong ligand instead. This might be the case if the cFe is partitioned into a ligand pool with no effective “free” ligand; in other words, the ligands binding the cFe do not have the capacity to take up any additional added Fe. It might only be possible to exchange Fe with this relatively “inert” pool if extremely long equilibration times are used, or if higher analytical windows are employed, which would “outcompete” all other natural ligands in the sample (Kogut and Voelker, 2001). It was not clear from our use of slightly higher analytical window whether this was the case (Figure 4).

Alternatively, a portion of the colloidal Fe could be nanoparticulate. , Dust-derived surface dFe tends to be colloidal, and while it could be bound by organic ligands of colloidal size, it could also be composed of nanoparticulate bits of dust physically eroded away or nanoparticulate Fe oxyhydroxides precipitated and/or aggregated *in situ* after aerosol Fe dissolves. This inorganic cFe would not be expected to adsorb to the electrochemical mercury drop or exchange Fe with the added ligand, and thus electrochemistry would interpret this cFe as

organically bound by a strong ligand. In this paper we modeled the predicted size partitioning of dFe using the size partitioning of the "excess" Fe-binding ligands; however, nanoparticulate Fe does not have an "excess" or "free" ligand pool. In other words, electrochemistry would not capture the "potential" to form nanoparticulate cFe that an unbound colloidal-sized ligand would. Thus, we would expect that if a significant portion of cFe was nanoparticulate, then we would see the same results that are observed in Figure 3: ligand partitioning predicts soluble-sized surface dFe while instead much of the dFe is actually colloidal (and inorganic).

Cullen *et al*. (2006) observed the same pattern (but to a lesser extent) in surface waters of the tropical North Atlantic, and they concluded that electrochemical methods were missing an "inert" pool of colloidal Fe ligands. Our observed data deviates much more substantially from the ligand-modeled data than Cullen *et al*. (2006) observed, but this may be explained by the higher analytical window employed by Cullen *et al*. (2006). A much higher competition strength was used in that study ($\alpha_{Fe(TAC)_x}$= 271) compared to those used here ($\alpha_{Fe(SA)_2}$= 100, 60), and in fact the higher analytical window in this study compares slightly better with the measured Fe partitioning (Table 3). This is a strong indication that at least some portion of the colloidal ligand pool may be very strong - either a very strong organic Fe-binding ligand of colloidal size or a relatively inert inorganic cFe species.

In addition to a chemical lability hindrance, a steric hindrance may also prevent these cFe ligands from being detected. In (1994), Mackey and Zirino presented the "onion model" in which trace metals in the ocean are bound by concentric layers of organic compounds held together by hydrogen and other coordination bonds. Thus, Fe may become sterically "trapped" inside a colloidal-sized organic matrix (which it does not have to bind particularly strongly to) that passes through our 0.2 µm filters and so is detected as dFe but is physically prevented from exchanging

with the added ligand. While they might bind Fe in nature given time and the physical mixing of the surface ocean, these same "onion" organic compounds in their unbound form in our samples might not bind Fe strongly enough during the time of electrochemical equilibration to reveal their true "binding potential" in nature.

Thus, our size partitioning Fe ligand results showed that in surface locations underlying the North African dust plume, the labile organic Fe-binding ligands detected by CLE-ACSV were overwhelmingly partitioned into the soluble size fraction and do not predict the colloidal Fe composition of dFe observed. This suggests that the "binding potential" of a significant colloidal Fe fraction is missed by current electrochemical techniques. We hypothesize that this "missing cFe" is composed either of nanoparticulate cFe (eroded dust fragments or *in situ* precipitated Fe oxyhydroxide aggregates) that has no way to demonstrate an "excess ligand"-like binding potential via electrochemistry or a kinetically-slow or sterically-hindered organic ligand of colloidal size. In short, attempting to unveil the chemical composition of new Fe upon external Fe inputs (such as dust fluxes) is challenging using electrochemical techniques because several colloidal Fe forms cannot fully demonstrate their true "binding potential" by CLE-ACSV. Further assessment and prediction of the composition and fate of dust-derived upper ocean dFe awaits new analytical methods that can chemically evaluate the binding environment of marine dFe species.

5. Conclusions

We evaluated the organic speciation of soluble (<10 kDa) and dissolved (<0.2 μm) Fe at a western and eastern station in the subtropical North Atlantic Ocean. We found that while the

majority of the dFe was colloidal sized (10 kDa - 0.2 µm), most of the excess organic ligands were soluble sized, indicating that the size partitioning of labile organic Fe-binding ligands does not directly predict the observed size partitioning of dFe. While our ultrafiltration methods did lose 35±27% of the organic ligands to the cross flow filtration membrane, the soluble ligands were inferred to permeate the membrane fully, and thus the filtration method was not the cause of the ligand and Fe size divergence. Two possible explanations were offered. First, our CLE-ACSV method could be missing some of the free colloidal sized ligands if they are kinetically limited to reaction times greater than the equilibration time of our method (2 hours). This could be caused by true kinetic limitation or steric hindrance, and these ligands would have to be 1) unbound in the sample (or CLE-ACSV would detect them), 2) have the potential to bind Fe in nature (presumably composing a portion of the existing cFe), but 3) bind Fe slower than the timescale of CLE-ACSV equilibration (which is why they were not detected). Alternatively, some of the cFe could be inorganically composed, which would not offer an "excess" ligand pool that could model and predict the dFe size partitioning accurately, as attempted here.

Acknowledgements

We would like to thank Gonzalo Carrasco and Pete Morton for help collecting and filtering seawater on the GA03 North Atlantic GEOTRACES cruise, and we thank Rene Boiteau and Dan Repeta for use of their deck pump and Chris Hayes for help at sea on the HOE-PhoR-II cruise to Station ALOHA. Finally, we thank C-MORE, the Chief Scientists of both cruises (Ed Boyle, Bill Jenkins, Greg Cutter, and Tara Clemente), and the officers and crew of the R/V *Kilo Moana* and the R/V *Knorr* for the opportunities to collect these samples at sea. J.N. Fitzsimmons was funded

by a National Science Foundation Graduate Research Fellowship (NSF Award #0645960), and research funding was provided by the National Science Foundation to E.A. Boyle (OCE #0926204 and OCE #0926197) and R.M. Bundy was partially funded by NSF OCE-0550302 and NSF OCE-1233733 to K. Barbeau and an NSF-GK12 graduate fellowship.

Table 1. Iron and ligand partitioning at stations 10 and 23 at the lower analytical window ($\alpha_{Fe(SA)_2}$ = 60).

Station	Size Fraction	Depth (m)	[Fe] nmol L^{-1}	+/-	[L_1] nmol L^{-1}	+/-	logK_1	+/-	[L_2] nmol L^{-1}	+/-	logK_2
10	soluble	3	0.089	0.003	1.51	0.13	12.78	0.03	1.10	0.02	10.91
10	dissolved	3	0.541	0.010	1.72	0.26	12.87	0.16	1.22	0.04	11.59
10	soluble	46	0.105	0.036	2.07	0.15	12.41	0.05	3.45	0.27	10.93
10	dissolved	46	0.642	0.003	2.40	0.62	12.32	0.18	4.33	0.01	10.68
10	soluble	62	0.098	0.002	1.68	0.01	12.71	0.74	4.58	0.54	11.31
10	dissolved	62	0.559	0.004	2.03	0.20	12.84	0.25	6.54	0.61	11.03
10	soluble	77	0.068	0.016	1.33	0.32	13.04	0.03	5.08	1.03	10.83
10	dissolved	77	0.439	0.008	2.78	0.37	12.15	0.12	5.91	4.08	10.84
10	soluble	84	0.071	0.004	1.80	0.02	12.64	0.16	4.64	1.31	11.67
10	dissolved	84	0.222	0.058	2.64	0.00	12.12	0.45	6.28	0.73	10.89
10	soluble	111	0.046	0.015	1.51	0.00	12.04	0.06	1.03	0.00	10.91
10	dissolved	111	0.154	0.006	1.65	0.00	12.67	0.23	1.71	0.19	11.05
23	soluble	3	0.094	0.004	1.26	0.25	12.60	0.25	4.84	0.29	11.19
23	dissolved	3	0.441	0.005	1.87	0.58	12.88	0.36	5.12	0.70	11.26
23	soluble	51	0.032	0.007	1.65	0.34	12.12	0.03	5.29	0.57	10.85
23	dissolved	51	0.347	0.002	1.76	0.25	12.62	0.14	6.69	2.14	10.99
23	soluble	77	0.025	0.007	1.01	0.08	12.51	0.69	7.25	0.21	10.57
23	dissolved	77	0.122	0.005	1.34	0.03	13.13	0.19	7.55	0.51	10.59
23	soluble	129	0.065	0.002	1.26	0.21	12.80	0.08	4.37	0.07	10.84
23	dissolved	129	0.344	0.009	1.93	0.03	12.64	0.27	4.88	4.86	10.87

Table 2. Iron and ligand partitioning at stations 10 and 23 at the higher analytical window ($\alpha_{Fe(SA)_2}$= 100).

Station	Size Fraction	Depth (m)	[Fe] nmol L^{-1}	+/-	[L_1] nmol L^{-1}	+/-	logK_1	+/-	[L_2] nmol L^{-1}	+/-	logK_2	+
10	soluble	3	0.089	0.003	1.14	0.03	12.74	0.04	0.91	0.14	11.86	0.0
10	dissolved	3	0.541	0.010	1.47	0.05	13.44	0.18	5.60	0.16	11.27	0.0
10	soluble	46	0.105	0.036	2.27	0.04	13.08	0.03	1.09	0.22	11.82	0.2
10	dissolved	46	0.642	0.003	2.81	0.20	12.59	0.17	4.13	0.19	11.13	0.0
10	soluble	62	0.098	0.002	1.56	0.01	12.31	0.30	4.92	0.01	11.24	0.0
10	dissolved	62	0.559	0.004	2.34	0.02	12.29	0.00	6.38	0.09	11.29	0.0
10	soluble	77	0.068	0.016	1.59	0.04	12.75	0.05	4.89	0.02	11.21	0.2
10	dissolved	77	0.439	0.008	2.24	0.18	12.44	0.21	5.25	0.40	10.98	0.4
10	soluble	84	0.071	0.004	2.04	0.03	12.14	0.17	3.22	0.70	11.48	0.0
10	dissolved	84	0.222	0.058	3.04	0.16	12.08	0.17	4.61	0.21	11.28	0.0
10	soluble	111	0.046	0.015	1.98	0.01	12.49	0.16	1.52	0.14	11.49	0.0
10	dissolved	111	0.154	0.006	2.01	0.13	12.54	0.11	3.70	0.50	11.32	0.2
23	soluble	3	0.094	0.004	1.96	0.05	12.18	0.03	1.57	0.48	11.36	0.1
23	dissolved	3	0.441	0.005	2.00	0.05	12.83	0.04	3.02	0.03	11.56	0.0
23	soluble	51	0.032	0.007	1.10	0.10	12.70	0.10	5.52	0.20	10.81	0.0
23	dissolved	51	0.347	0.002	1.16	0.77	13.04	1.03	5.73	0.40	11.52	0.2
23	soluble	77	0.025	0.007	1.65	0.23	12.11	0.00	2.26	0.07	11.10	0.0
23	dissolved	77	0.122	0.005	1.96	0.08	13.21	0.20	2.52	0.05	11.80	0.0
23	soluble	129	0.065	0.002	2.89	0.05	12.18	0.01	3.46	0.30	10.93	0.4
23	dissolved	129	0.344	0.009	2.92	0.16	12.20	0.05	3.90	0.97	10.91	0.1

Table 3. Modeled and measured iron and ligand partitioning according to Equation 3 for stations 10 and 23.

Station	Size Fraction	Depth	[Fe] nmol L^{-1}	$\alpha_{Fe(SA)2}$	$\log\alpha_{FeL}$	Modeled $\alpha_{sol}/\alpha_{diss}$	Measured Fe_{sol}/Fe_{diss}	$\alpha_{Fe(SA)2}$	$\log\alpha_{FeL}$	Modeled $\alpha_{sol}/\alpha_{diss}$	Measured Fe_{sol}/Fe_{diss}
10	soluble	3	0.089	60	13.94	0.95	0.16	100	13.81	0.24	0.16
10	dissolved	3	0.541	60	13.96			100	14.43		
10	soluble	46	0.105	60	13.72	1.36	0.16	100	14.43	2.95	0.16
10	dissolved	46	0.642	60	13.59			100	13.96		
10	soluble	62	0.098	60	13.95	0.83	0.18	100	13.58	0.81	0.18
10	dissolved	62	0.559	60	14.03			100	13.67		
10	soluble	77	0.068	60	14.15	3.84	0.16	100	13.97	1.71	0.16
10	dissolved	77	0.439	60	13.56			100	13.74		
10	soluble	84	0.071	60	13.98	2.64	0.32	100	13.57	0.86	0.32
10	dissolved	84	0.222	60	13.56			100	13.63		
10	soluble	111	0.046	60	13.22	0.23	0.30	100	13.81	0.93	0.30
10	dissolved	111	0.154	60	13.85			100	13.84		
23	soluble	3	0.094	60	13.73	0.46	0.21	100	13.51	0.28	0.21
23	dissolved	3	0.441	60	14.07			100	14.06		
23	soluble	51	0.032	60	13.40	0.38	0.09	100	13.76	0.53	0.09
23	dissolved	51	0.347	60	13.82			100	14.03		
23	soluble	77	0.025	60	13.54	0.21	0.20	100	13.38	0.10	0.20
23	dissolved	77	0.122	60	14.22			100	14.39		
23	soluble	129	0.065	60	13.89	1.08	0.19	100	13.66	1.04	0.19
23	dissolved	129	0.344	60	13.86			100	13.64		

Table 4. Fe and Fe-binding ligand mass balance using cross flow filtration at 15 m depth at Station ALOHA in the Pacific Ocean.

Sample	**[Fe] nM**	**+/-**	**$[L]_T$ nM**	**+/-**	**[eL] nM**	**+/-**
Measured permeate ("soluble"), <10 kDa	0.039	0.008	0.300	0.008	0.262	0.011
Measured retentate	0.153	0.002	0.552	0.072	0.399	0.072
Measured CFF feed ("dissolved), <0.2 µm	0.176	0.014	0.654	0.032	0.478	0.035
Calculated colloidal (Equations 1 and 2)	0.057	0.008	0.126	0.072	0.068	0.073
Calculated soluble+colloidal	0.096	0.012	0.426	0.072	0.330	0.073
% Recovery	**54.5%**	*27%*	**65.1%**	*27%*	**69.1%**	*34%*

Table 5. Mass balance-calculated colloidal ligand characteristics (at $\alpha_{Fe(SA)_2}$ = 60) and the additional "kinetically-inhibited" colloidal L_2 concentrations required to explain the observed dFe size partitioning at equilibrium.

Sta.	**Depth (m)**	**[cFe] nM**	**+/-**	**[Coll L_1] nM**	**+/-**	**Coll logK_1**	**[Coll L_2] nM**	**+/-**	**Coll logK_2**	**Additional [Coll L_2] nM**
10	3	0.452	0.010	0.21	0.29	13.22	0.12	0.05	12.50	13.81
10	46	0.537	0.036	0.33	0.63	--	0.88	0.27	--	--
10	62	0.461	0.005	0.35	0.20	13.19	1.96	0.81	--	--
10	77	0.371	0.018	1.46	0.49	--	0.83	4.21	10.89	59.57
10	84	0.152	0.058	0.84	0.02	--	1.65	1.50	--	--
10	111	0.108	0.016	0.14	0.00	13.63	0.68	0.19	11.20	-0.33
23	3	0.347	0.006	0.61	0.63	13.17	0.28	0.76	11.83	1.63
23	51	0.316	0.007	0.11	0.42	13.67	1.40	2.22	11.31	4.72
23	77	0.097	0.009	0.33	0.09	13.65	0.30	0.55	10.96	0.03
23	129	0.279	0.009	0.67	0.21	11.85	0.51	4.86	11.07	7.63

Figure 1. Sampling locations along the US-GEOTRACES 2011 transect for iron and iron-binding ligand partitioning studies.

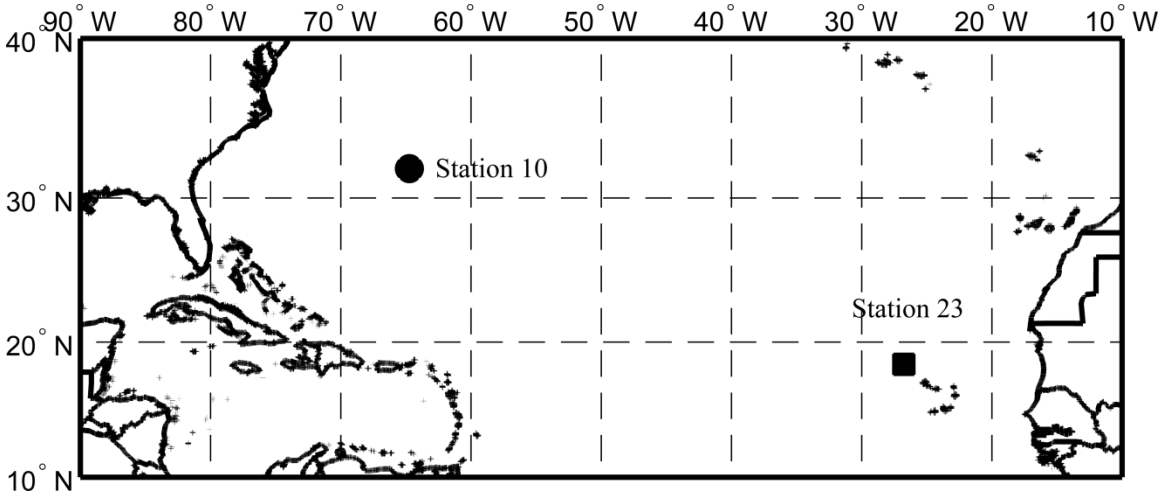

Figure 2. Hydrography of the two North Atlantic study sites. The CTD traces from relevant sample depths are indicated in (a) for station 10 near Bermuda and (b) for station 23 near Cape Verde.

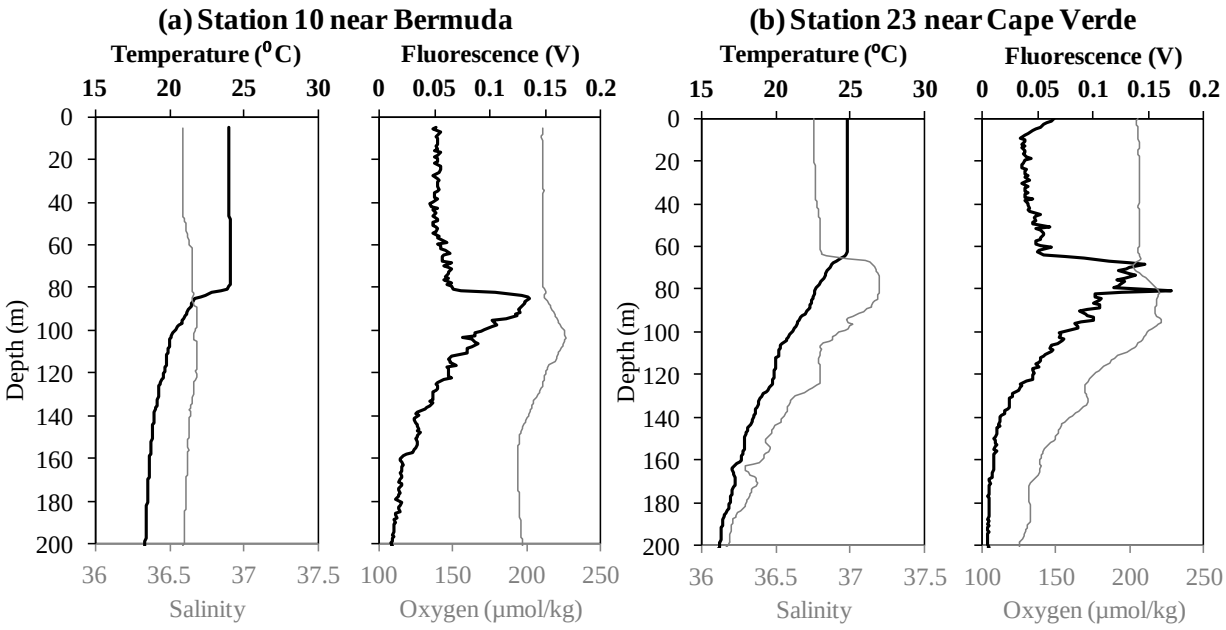

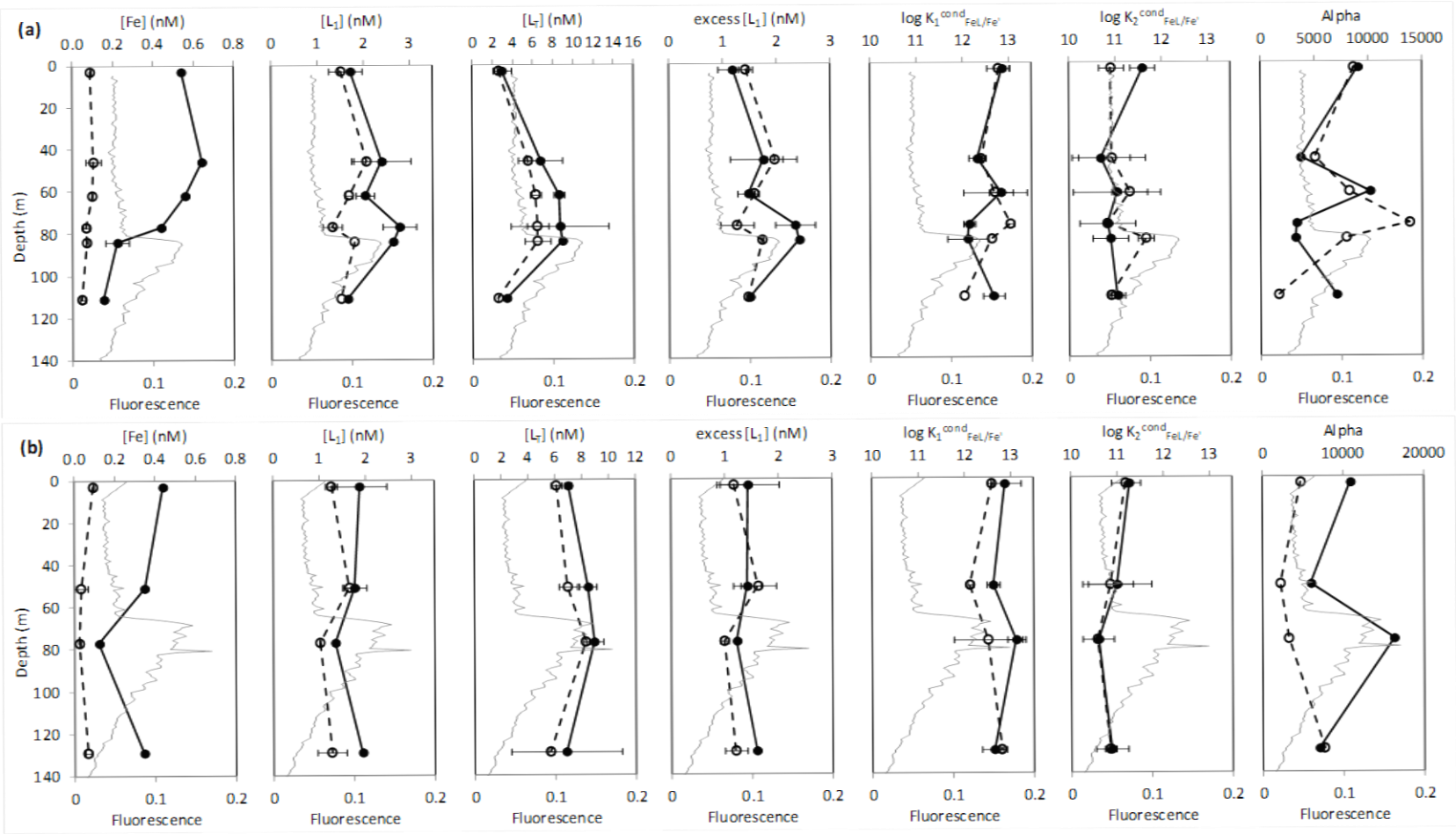

Figure 3: The partitioning of dFe and dissolved Fe-binding ligands in the dissolved (<0.2 µm, solid circles, solid line) and soluble (<10 kDa, open circles, dotted lines) at (a) station 10 (BATS) and (b) station 23 (near Cape Verde). The gray line is the fluorescence trace, and the maximum fluorescence is designated as the deep chlorophyll maximum (DCM). All error bars are ±1 standard deviation.

Figure 4. Measured sFe/dFe vs. modeled sFe/dFe at station 10 (near Bermuda, filled circles) and station 23 (near Cape Verde, crosses) at $\alpha_{Fe(SA)_2}$ = 60 and 100 (A and B, respectively). Modeled sFe/dFe was derived by dividing $\alpha_{soluble}/\alpha_{dissolved}$.

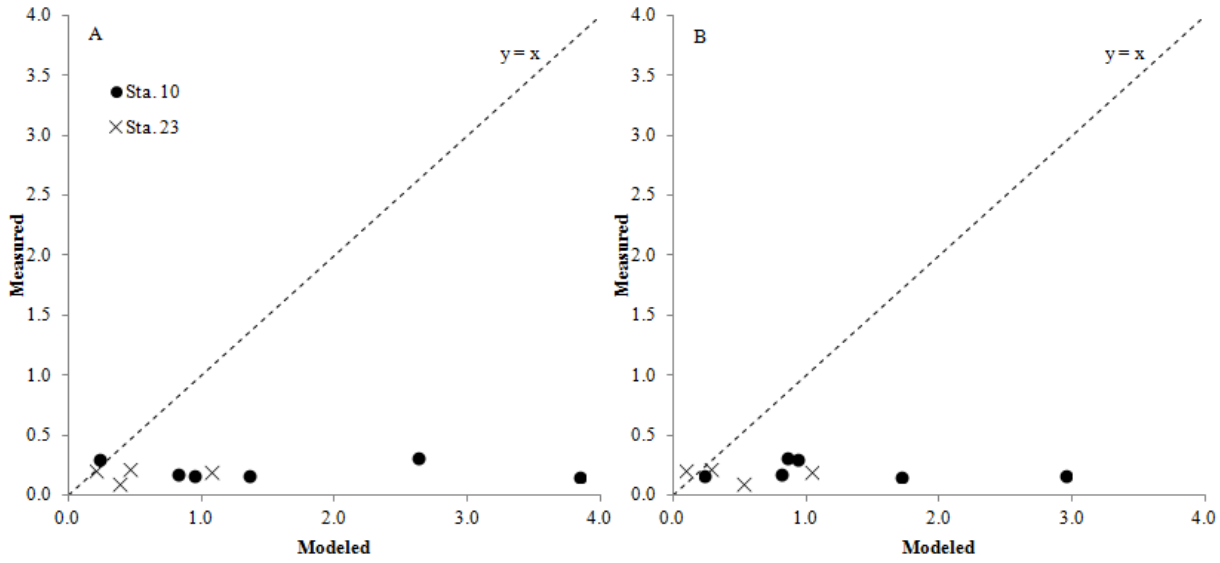

References

Aguilar-Islas, A.M. and Mehalek, A., 2013. Aerosol Fe solubility from field and lab-based leaching protocols, U.S. GEOTRACES post-cruise data workshop, Old Dominion University, Norfolk, VA.

Aguilar-Islas, A.M., Wu, J., Rember, R., Johansen, A.M. and Shank, L.M., 2010. Dissolution of aerosol-derived iron in seawater: Leach solution chemistry, aerosol type, and colloidal iron fraction. Marine Chemistry, 120(1-4): 25-33.

Baker, A.R. and Croot, P.L., 2010. Atmospheric and marine controls on aerosol iron solubility in seawater. Marine Chemistry, 120: 4-13.

Bergquist, B.A., Wu, J. and Boyle, E.A., 2007. Variability in oceanic dissolved iron is dominated by the colloidal fraction. Geochimica Et Cosmochimica Acta, 71(12): 2960-2974.

Boye, M. et al., 2010. Significant portion of dissolved organic Fe complexes in fact is Fe colloids. Marine Chemistry, 122(1-4): 20-27.

Buck, K.N., Lohan, M.C., Berger, C.J.M. and Bruland, K.W., 2007. Dissolved iron speciation in two distinct river plumes and an estuary: Implications for riverine iron supply. Limnology & Oceanography, 52(2): 843-855.

Chen, M., Dei, R.C.H., Wang, W.-X. and Guo, L., 2003. Marine diatom uptake of iron bound with natural colloids of different origins. Marine Chemistry, 81(3-4): 177-189.

Chen, M. and Wang, W.X., 2001. Bioavailability of natural colloid-bound iron to marine plankton: Influences of colloidal size and aging. Limnology & Oceanography, 46(8): 1956-1967.

Chever, F. et al., 2010. Physical speciation of iron in the Atlantic sector of the Southern Ocean along a transect from the subtropical domain to the Weddell Sea Gyre. Journal of Geophysical Research, 115(C10): C10059.

Conway, T.M. and John, S.G., in press. Quantification of sources of dissolved iron to the North Atlantic Ocean. Nature.

Cullen, J.T., Bergquist, B.A. and Moffett, J.W., 2006. Thermodynamic characterization of the partitioning of iron between soluble and colloidal species in the Atlantic Ocean. Marine Chemistry, 98(2-4): 295-303.

Cutter, G.A. and Bruland, K.W., 2012. Rapid and noncontaminating sampling system for trace elements in a global ocean surveys. Limnology & Oceanography: Methods, 10: 425-436.

Fitzsimmons, J.N. and Boyle, E.A., 2014a. Assessment and comparison of Anopore and cross flow filtration methods for the determination of dissolved iron size fractionation into soluble and colloidal phases in seawater. Limnology & Oceanography: Methods, 12: 244-261.

Fitzsimmons, J.N. and Boyle, E.A., 2014b. Both soluble and colloidal iron phases control dissolved iron variability in the tropical North Atlantic Ocean. Geochimica et Cosmochimica Acta, 125: 539-550.

Fitzsimmons, J.N. and Boyle, E.A., in review. Both soluble and colloidal iron phases control dissolved iron variability in the tropical North Atlantic Ocean. Geochimica et Cosmochimica Acta.

Fitzsimmons, J.N. et al., in review. Partitioning of dissolved iron and iron isotopes into soluble and colloidal phases along the GA03 GEOTRACES North Atlantic Transect. Deep-Sea Research II U.S. GEOTRACES North Atlantic Special Issue.

Gledhill, M., 2007. The determination of heme b in marine phyto- and bacterioplankton. Marine Chemistry, 103(3-4): 393-403.

Gledhill, M. and Buck, K.N., 2012. The organic complexation of iron in the marine environment: a review. Frontiers in Microbiology, 3: 69.

Gledhill, M. and van den Berg, C.M.G., 1994. Determination of complexation of iron(III) with natural organic ligands in seawater using cathodic stripping voltammetry. Marine Chemistry, 47: 41-54.

Hassler, C.S., Alasonati, E., Mancuso Nichols, C.A. and Slaveykova, V.I., 2011a. Exopolysaccharides produced by bacteria isolated from the pelagic Southern Ocean: Role in Fe binding, chemical reactivity, and bioavailability. Marine Chemistry, 123: 88-98.

Hassler, C.S., Schoemann, V., Nichols, C.M., Butler, E.C.V. and Boyd, P.W., 2011b. Saccharides enhance iron bioavailability to Southern Ocean phytoplankton. Proceedings of the National Academy of Sciences, 108(3): 1076-1081.

Hopkinson, B.M., Roe, K.L. and Barbeau, K.A., 2008. Heme uptake by *Microsilla marina* and evidence for heme uptake systems in the genomes of diverse marine bacteria. Applied and Environmental Microbiology, 74(20): 6263-6270.

Jickells, T.D. et al., 2005. Global iron connections between desert dust, ocean biogeochemistry, and climate. Science, 308(5718): 67-71.

Kogut, M.B. and Voelker, B.M., 2001. Strong copper-binding behavior of terrestrial humic substances in seawater. Environmental Science and Technology, 35(6): 1149-1156.

Laglera, L.M. and van den Berg, C.M.G., 2009. Evidence for geochemical control of iron by humic substances in seawater. Limnology & Oceanography, 54(2): 610-619.

Lee, J.-M. et al., 2011. Analysis of trace metals (Cu, Cd, Pb, and Fe) in seawater using single batch Nitrilotriacetate resin extraction and isotope dilution inductively coupled plasma mass spectrometry. Analytica Chimica Acta, 686: 93-101.

Liu, X. and Millero, F.J., 2002. The solubility of iron in seawater. Marine Chemistry, 77: 43-54.

Mackey, D.J. and Zirino, A., 1994. Comments on trace metal speciation in seawater or do "onions" grow in the sea? Analytica Chimica Acta, 284: 635-647.

Mahowald, N. et al., 2005. Atmospheric global dust cycle and iron inputs to the ocean. Global Biogeochemical Cycles, 19: GB4025.

Mantoura, R.F.C. and Riley, J.P., 1975. The use of gel filtration in the study of metal binding by humic acids and related compounds. Analytica Chimica Acta, 78: 193-200.

Mawji, E. et al., 2011. Production of siderophore type chelates in Atlantic Ocean water enriched with different carbon and nitrogen sources. Marine Chemistry, 124: 90-99.

Millero, F.J., 1998. Solubility of Fe(III) in seawater. Earth and Planetary Science Letters, 154: 323-329.

Moore, J.K., Doney, S.C., Glover, D.M. and Fung, I.Y., 2002. Iron cycling and nutrient-limitation patterns in surface waters of the World Ocean. Deep Sea Research Part II: Topical Studies in Oceanography, 49(1-3): 463-507.

Morel, F.M.M., Kustka, A.B. and Shaked, Y., 2008. The role of unchelated Fe in the iron nutrition of phytoplankton. Limnology & Oceanography, 53(1): 400-404.

Morel, F.M.M., Milligan, A.J. and Saito, M.A., 2003. Marine Bioinorganic Chemistry: The Role of Trace Metals in the Oceanic Cycles of Major Nutrients. In: K.K. Turekian and H.D. Holland (Editors), Treatise On Geochemistry. Elsevier Science Ltd., Cambridge, United Kingdom, pp. 113-143.

Nishioka, J. et al., 2003. Size-fractionated iron distributions and iron-limitation processes in the subarctic NW Pacific. Geophysical Research Letters, 30(14): 1730.

Nishioka, J., Takeda, S., Wong, C.S. and Johnson, W.K., 2001. Size-fractionated iron concentrations in the northeast Pacific Ocean: distribution of soluble and small colloidal iron. Marine Chemistry, 74(2-3): 157-179.

Reitmeyer, R., Powell, R.T., Landing, W.M. and Measures, C.I., 1996. Colloidal aluminum and iron in seawater: An intercomparison between various cross-flow ultrafiltration systems. Marine Chemistry, 55: 75-91.

Rich, H.W. and Morel, F.M.M., 1990. Availability of well-defined iron colloids to the marine diatom *Thalassiosira weissflogii*. Limnology & Oceanography, 35(3): 652-662.

Rue, E.L. and Bruland, K.W., 1995. Complexation of iron(III) by natural organic ligands in the Central North Pacific as determined by a new competitive ligand equilibration/adsorptive cathodic stripping voltammetric method. Marine Chemistry, 50(1-4): 117-138.

Ružić, I., 1982. Theoretical aspects of the direct titration of natural waters and its information yield for trace metal speciation. Analytica Chimica Acta, 140: 99-113.

Scatchard, G., 1949. The attractions of proteins for small molecules and ions. Annals of the New York Academy of Sciences, 51: 660-672.

Shaked, Y., Kustka, A.B. and Morel, F.M.M., 2005. A general kinetic model for iron acquisition by eukaryotic phytoplankton. Limnology & Oceanography, 50(3): 872-882.

Shelley, R.U., Morton, P.L. and Landing, W., in review. Elemental composition of North Atlantic aerosols (US GEOTRACES). Deep-Sea Research II U.S. GEOTRACES North Atlantic Special Issue.

Sunda, W.G., 2012. Feedback interactions between trace metal nutrients and phytoplankton in the ocean. Frontiers in Microbiology, 3: 204.

Talley, L.D., Pickard, G.L., Emery, W.J. and Swift, J.H., 2011. Descriptive Physical Oceanography. Elsevier Ltd.

Thuróczy, C.E. et al., 2010. Speciation of Fe in the Eastern North Atlantic Ocean. Deep Sea Research Part I: Oceanographic Research Papers, 57(11): 1444-1453.

Ussher, S.J. et al., 2010. Distribution of size fractionated dissolved iron in the Canary Basin. Marine Environmental Research, 70(1): 46-55.

van den Berg, C.M.G., 1982. Determination of copper complexation with natural organic ligands in sea water by equilibrium with MnO_2: I. Theory. Analytica Chimica Acta, 11: 307-312.

van den Berg, C.M.G., 1995. Evidence for organic complexation of iron in seawater. Marine Chemistry, 50(1-4): 139-157.

Velasquez, I. et al., 2011. Detection of hydroxamate siderophores in coastal and sub-Antarctic waters off the South Eastern coast of New Zealand. Marine Chemistry, 126: 97-107.

von der Heyden, B.P., Roychoudhury, A.N., Mtshali, T.N., Tyliszczak, T. and Myneni, S.C.B., 2012. Chemically and Geographically Distinct Solid-Phase Iron Pools in the Southern Ocean. Science, 338(6111): 1199-1201.

Vraspir, J. and Butler, A., 2009. Chemistry of marine ligands and siderophores. Annual Review of Marine Science, 1: 43-63.

Wang, W.X. and Dei, R.C.H., 2003. Bioavailability of iron complexed with organic colloids to the cyanobacteria *Synechococcus* and *Trichodesmium*. Aquatic Microbial Ecology, 33: 247-259.

Wells, M.L., 2003. The level of iron enrichment required to initiate diatom blooms in HNLC waters. Marine Chemistry, 82(1-2): 101-114.

Wells, M.L. and Goldberg, E.D., 1992. Marine submicron particles. Marine Chemistry, 40: 5-18.

Worthington, L.V., 1959. The 18 ° water in the Sargasso Sea. Deep-Sea Research, 5: 297-305.

Wu, J., Boyle, E.A., Sunda, W.G. and Wen, L., 2001. Soluble and colloidal iron in the oligotrophic North Atlantic and North Pacific. Science, 293: 847-849.

Wu, J. and Luther, G.W., 1995. Complexation of Fe(III) by natural organic ligands in the Northwest Atlantic Ocean by a competitive ligand equilibration method and a kinetic approach. Marine Chemistry, 50(1-4): 159-177.

Poster presentation at C-MORE (Hawaii; USA 2014)